ELECTROMECHANICAL PERISTALTIC PUMPING

Reed Robert Burn

ELECTROMECHANICAL PERISTALTIC PUMPING

BY

REED ROBERT BURN

Lieutenant Commander, United States Navy

B.S., United States Naval Academy
1961

Submitted to the Department of Naval Architecture and Marine Engineering in Partial Fulfillment of the Requirements of the Master of Science Degree in Electrical Engineering and the Professional Degree, Naval Engineer

at the

MASSACHUSETTS INSTITUTE OF TECHNOLOGY

May, 1970

ELECTROMECHANICAL PERISTALTIC PUMPING

by

Reed Robert Burn

Submitted to the Department of Naval Architecture and Marine Engineering of May 21, 1970, in partial fulfillment of the requirements for the Master of Science Degree in Electrical Engineering and the Professional Degree, Naval Engineer.

ABSTRACT

Historically, peristalsis, the rhythmic, traveling wave like pumping of bodily organs such as the ureter, has been mechanically simulated by the extended longitudinal motion of rollers squeezing fluid along a flow channel. Blood pumps are an example. The experimental work associated with this thesis has developed a peristaltic pump wherein pumping is produced by the limited transverse motion of electromechanical transducers. The transducers are arranged in a line and excitation is time phased so that their sequential transverse motions produce a traveling deflection wave along the pump flow tube.

The pump is a simple device made from transformer cores. Each transformer serves as a transducer; the "E", with windings on the center leg, provides AC and DC excitation; the "I" serves as the actuator which squeezes the pump tube and produces flow. The magnetic action is much like a solenoid in that the "E" and "I" serve as a magnetic circuit and the magnetic field in the air gaps produces the tube squeezing force.

The theory developed in the thesis involves the electromechanical characteristics of each pump transducer and the fluid mechanical flow characteristics for the pump. The final tying together of theory and experiment is a comparison of theoretical pump pressure-flow characteristic curves and experimental pump operating points. Operating points do conform fairly well to the pressure-flow characteristics, but insufficient operating points were determined to state that the pressure-flow curves accurately predict pump operation.

Production of peristaltic pumping by transverse deflections has great potential value. If a peristaltic pump is ever to be used as a replacement for an organ of the body, longitudinal rollers are not practical. The transverse deflection pump is simple and also might be miniaturized. In place of transformers, piezoelectric crystals could be used as transducers. With a DC voltage excitation, crystals could produce great forces over short displacements. Miniaturization and improvements as recommended in the thesis are worthwhile areas for future experimentation and development.

ACKNOWLEDGEMENTS

The author wishes to express his appreciation to Professor James R. Melcher, Department of Electrical Engineering, Massachusetts Institute of Technology, for providing the topic of the thesis and for his help in its development.

Financial support for this research was provided by the United States Navy and the National Aeronautics and Space Administration under contract number NGL-22-009-014.

CONTENTS

SYMBOLS

Notation	Name and Unit of the Symbol
a	Transducer outer leg thickness, meters
b	Transducer exciter center leg thickness, meters
B	Magnetic flux density, webers/m^2
c	Phase velocity, m/sec
d	Transducer exciter width, meters
D	Damping coefficient
∇	Vector differential operator
f	Frequency, hertz
f_e	Electric force, newtons
f_p	Fluid pressure force, newtons
f_s	Spring force, newtons
ϕ	Magnetic flux, webers
g	Gravity acceleration, m/sec^2
h	Normalized channel width, r/R
H	Magnetic field intensity, amp-turns/m
H_s	Pump suction head, meters
H_d	Pump discharge head, meters
i	Time varying current, amps
I	Steady state current, amps
j	$(-1)^{\frac{1}{2}}$
J	Current Density, amps/m^2
k	Wave number, $2\pi/\lambda$
K	Spring constant, newtons/m

Notation	Name and Unit of the Symbol
l	Actuator width, $\lambda/4$, meters
L	Inductance, henries
λ	Wavelength, meters
M	Actuator mass, kg
μ	Dynamic viscosity, newton-sec/m^2
μ_o	Permitivity of free space, henries/m
N	Exciter winding turns, turns
ν	Kinematic viscosity, μ/ρ
P	Fluid pressure, newtons/m^2
ΔP_λ	Pressure rise over a wavelength, Newtons/m^2
$\underline{\Delta P}$	Normalized pressure rise, $\frac{R^2 \Delta P_\lambda}{6\mu\lambda c}$
Q	Instantaneous fluid flow, m^3/sec
$\langle Q \rangle$	Time average fluid flow, m^3/sec
$\underline{\langle Q \rangle}$	Normalized time average fluid flow, $\frac{\langle Q \rangle}{Rc}$
r	Time varying component of channel width, meters
R	Equilibrium channel width, meters
ρ	Fluid density, kg/m^3
t	Time, sec
T	Maxwell stress tensor, Newtons/m^2
v	Fluid velocity, m/sec
w	Channel width, meters
W_m	System energy, watts
W'_m	System co-energy, watts
x	Spatial co-ordinate

Notation	Name and Unit of the Symbol
X	Transducer gap width, meters
X_s	Tube support thickness, meters
y	Spatial co-ordinate
z	Spatial co-ordinate
ω	Frequency, $2\pi f$, radians/sec

CHAPTER I

INTRODUCTION

Peristalsis is the rhythmic motion of the walls of the alimentary canal, the ureter, and other hollow organs of the body, consisting of traveling wave contractions and dilations that move the contents of the tube onward. Outside the body, peristaltic pumping can be achieved by mechanically squeezing a fluid filled channel or tube in a traveling wave manner.

The potential value of such a device must be apparent. In industry, the need often exists to pump fluids without having the fluid touch the pump apparatus, as in the case of blood and caustic chemicals. The peristaltic pump enables the insertion of a fluid carrying tube into the pump with no actual contact between the fluid and the pump mechanism. In addition, if such a device could be miniaturized, it might be inserted into the body to create artificial body functions when natural functions have failed.

All present peristaltic pumps rely on transverse pump tube deflections, which travel longitudinally, to create fluid motion.[1,2,3] Deflection is generally produced by a mechanical roller which moves along the tube, squeezes it, and pushes the fluid onward. Electrical forces are involved only in that an electric motor produces the force which causes the longitudinal mechanical motion.

This investigation deals with a different class of electromechanical devices. In general, mechanical motion is purely transverse and electric forces are directly related to pump tube deflections.[4] Schematic representations of such devices are shown in Figure 1.1. In Figure 1.1.a, the channel walls form a continuum electromechanical transducer. The source of electrical force is a current sheet which is wound similar to the windings in an electric motor field and which produces a sinusoidal traveling wave. If the channel is an elastic tube, the continuum transducer can be approximated by arranging a large number of discrete magnetic segments on top of the tube. Their response to the traveling magnetic wave will cause tube deflections.

Figure 1.1.b represents a peristaltic pump which also moves purely transversely, but the sources of tube deflection are discrete transducers rather than an electromechanical continuum. The schematic shows each transducer being one quarter wavelength. In order to produce a single wavelength of a traveling wave, as illustrated, each transducer excitation must be phase shifted ninety degrees from its predecessor. The number of discrete transducers per wavelength can be increased as desired, provided they are properly excited. In the limit of many transducers, the discrete pump approaches being a continuum.

SCHEMATIC REPRESENTATION OF A TRAVELING WAVE PERISTALTIC PUMP

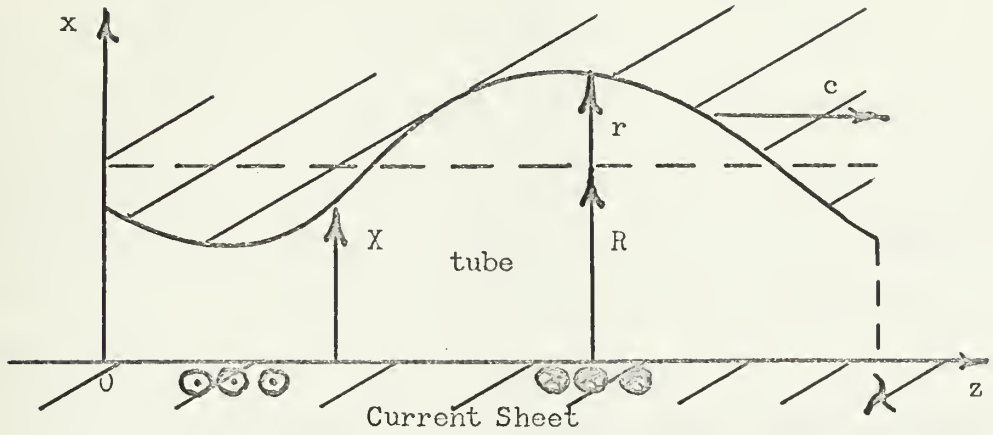

a.

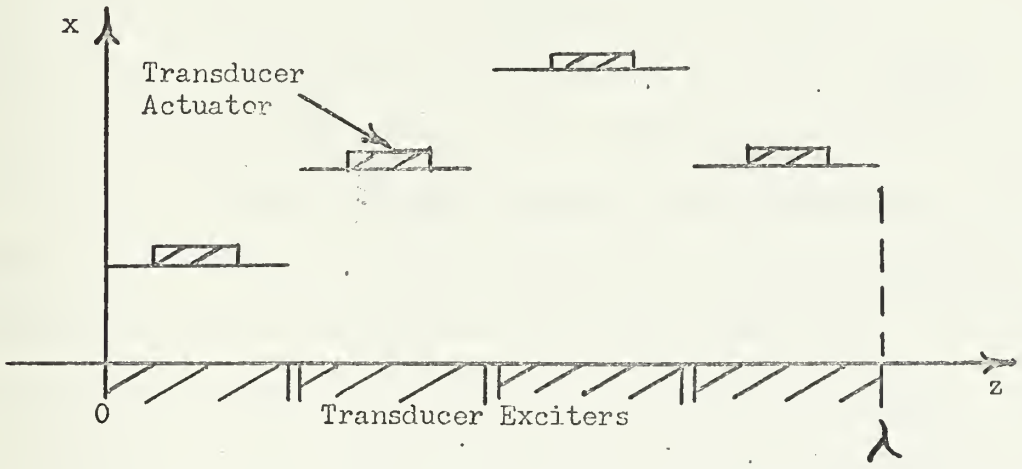

b.

$\lambda >> r$

$\lambda >> R$

Pressure = P(z)

Velocity = $V_z(x)$

r = r(z)

Figure 1.1

In both representations, Figures 1.1.a and 1.1.b, the electric force which causes tube deflection is a function of the gap width, X, between the actuator and the exciter. It will be shown that this relationship produces a mechanical instability which causes the discrete configuration of Figure 1.1.b to operate in an on-off, that is, channel open-channel cut off, mode.

The analytical model for the pump is based upon the physical situation most likely to be encountered where peristaltic flow exists.[5] Transverse tube dimensions are small compared to a wavelength of the traveling wave. Transverse velocities and pressure gradients are small compared with longitudinal ones. The pressure in the tube is assumed to be instantaneously uniform over each cross section. The fluid density and viscosity are assumed to be constant. The Reynold's number is assumed to be low enough so that flow is viscous. In order to insure the validity of a viscous model, Reynold's numbers should be less than one.[6]

The tube walls move in the transverse direction only. The traveling wave shape will be analyzed as both sinusoidal and square.[7,8] Pumping does not seem to be sensitive to the shape of the wave, but specific values of flow rates are sensitive to the type of tube deflection.

The pump developed for investigation in this work is

shown in Figure 1.2. It consists of four transducers which are excited to produce a single traveling wavelength along the pump tube. The tube is inserted between the transducer exciter and actuator. The actuator is supported by four springs, one at each corner, and by the fluid pressure in the tube passing underneath. The transducers have two exciter windings. One supplies direct bias current. The other supplies alternating current. The alternating current source is a sine-cosine potentiometer, the output of which is amplified through amplidynes to produce the desired low frequency current values. The phase shift in excitation between each transducer is ninety degrees.

The analysis of the pump is done step by step, starting with a single transducer and ending with the completed peristaltic pump.

In chapter two, the inductance of a single transducer, the supporting spring constant, and the electric forces exerted on a transducer as it will appear in the pump are determined. Then the time variation of a single transducer and the set of four transducers in sequence is ascertained for various direct and alternating current excitations. The frequency of alternating current is arbitrary except that the Reynold's number is directly proportional to frequency. Lower Reynold's numbers result from lower frequencies. The lowest possible Reynold's number is desired to have viscous flow forces dominate

PERISTALTIC PUMP

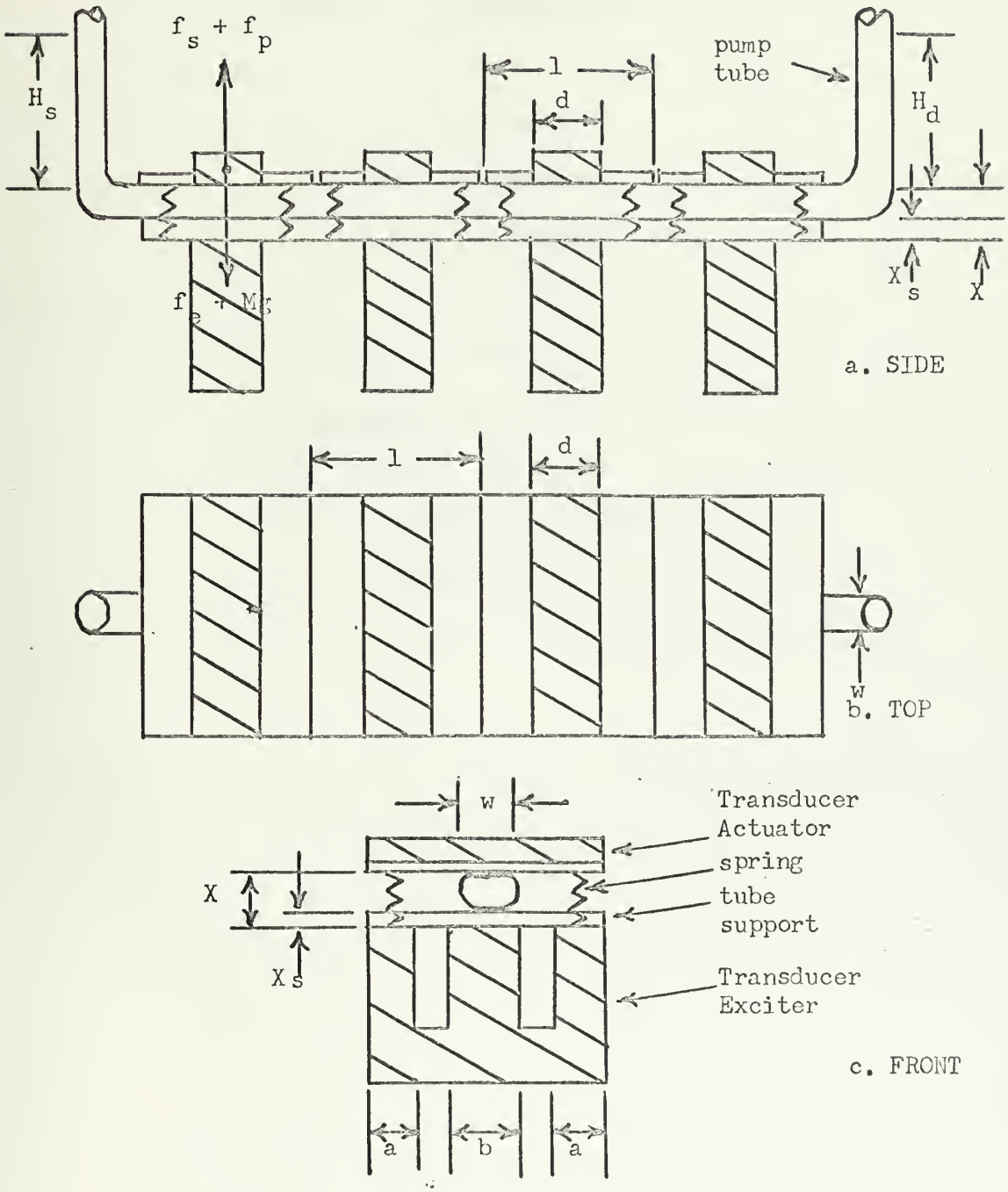

Figure 1.2

PERISTALTIC PUMP PARAMETERS

$a = 1.45 \times 10^{-2}$ meters

$b = 2.90 \times 10^{-2}$ meters

$d = 2.95 \times 10^{-2}$ meters

$l = 7.00 \times 10^{-2}$ meters

$N_{primary} = 500$ turns

$N_{secondary} = 26$ turns

$Xs = 1.73 \times 10^{-3}$ meters

w = variable tube width

X = variable gap width

Figure 1.3

inertial flow forces.

Once the transducers are analyzed individually, the peristaltic pump of which they are a part is analyzed as a whole in chapter three. First, an empirical expression for the pressure force exerted by the pump tube is obtained. Then a theoretical expression describing transducer actuator motion is determined. Finally, based on known actuator deflections, the pressure-flow characteristics of the pump are determined for a square traveling wave and a sinusoidal traveling wave description of tube deflections. The experimental operating points for the pump are compared to these characteristics.

Throughout chapters two and three, analytic work is immediately followed by test results. This is done because experimental results from some sections are used in following analytic work.

CHAPTER II

MAGNETIC TRANSDUCER ANALYSIS

2.1 Magnetic Transducer Inductance

2.1.1 Theoretical Inductance

The theoretical inductance of a single transducer is determined using lumped parameter electromechanical techniques.[9] Apply Ampere's law to the transducer as pictured in Figure 2.1a. The permeability of the exciter and actuator are assumed to be infinite. This requires that the magnetic field intensity, H, must be zero since the flux density, B, is finite and $B = \mu_0 H$. The only magnetic field is in the gaps between the exciter and the actuator.

$$\int_s \nabla X H \cdot n \, da = \int_s J \cdot n \, da \qquad 2.1a$$

Apply Stokes' theorem to obtain

$$\int_c H \cdot dl = \int_s J \cdot n \, da \qquad 2.1b$$

The contours for these integrals are indicated as dotted lines on Figure 2.1a. Integration yields

$$H_1 X + H_2 X = N I \qquad 2.2$$

Taking a surface that encloses the transducer actuator in

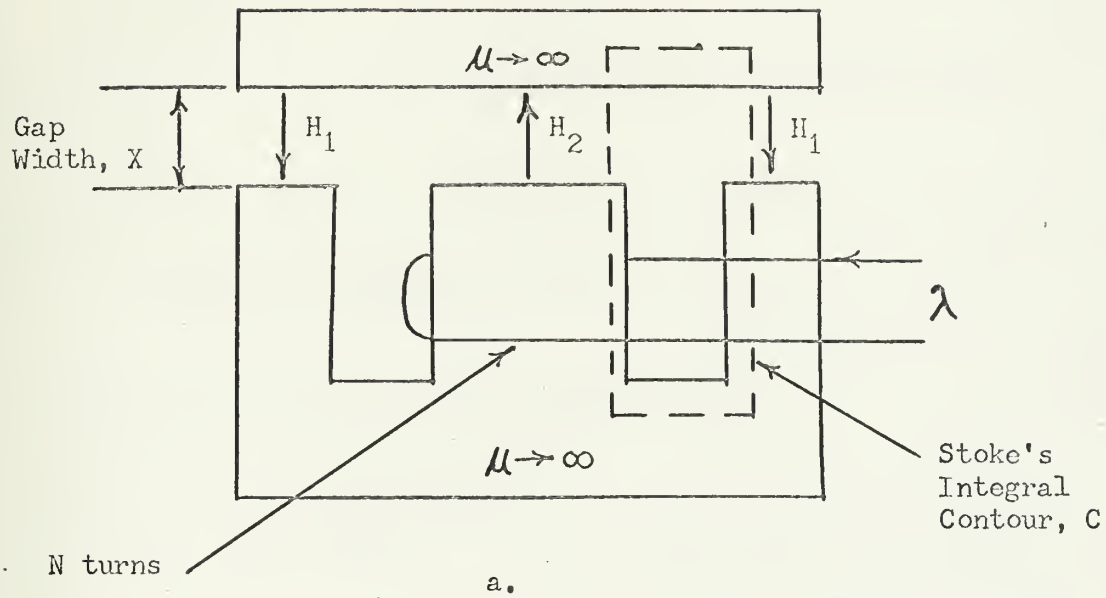
μ→∞
Gap
Width, X
H1
H2
H1
λ
μ→∞
Stoke's
Integral
Contour, C
N turns

a.

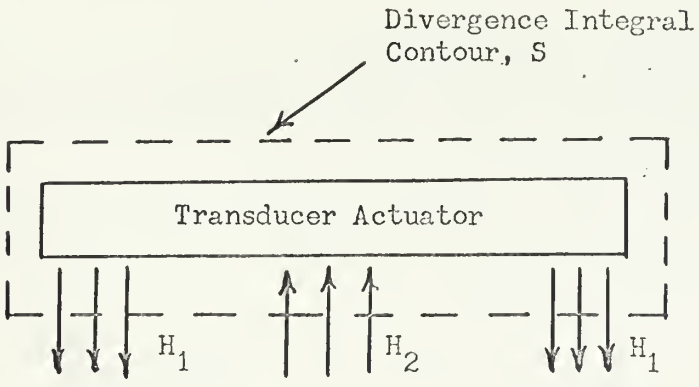
Divergence Integral
Contour, S
Transducer Actuator
H1
H2
H1

b.

Figure 2.1

Figure 2.1b, knowing that $\nabla \cdot B = 0$, integrating $\nabla \cdot B$ over the enclosed volume, and applying the divergence theorem yields

$$\int_s B \cdot n \, da = 0 \qquad 2.3$$

In terms of the magnetic field penetrating the enclosing surface, this becomes

$$2\mu_0 H_1 \, a \, d - \mu_0 H_2 \, b \, d = 0 \qquad 2.4$$

Solve equations 2.2 and 2.4 simultaneously.

$$H_1 = \frac{b}{2a + b} \frac{N I}{X} \qquad 2.5$$

$$H_2 = \frac{2a}{2a + b} \frac{N I}{X} \qquad 2.6$$

The total flux through the center leg is

$$\phi = \mu_0 H_2 \, b \, d \qquad 2.7$$

$$= \frac{2 \mu_0 N I \, a \, b \, d}{X (2a + b)} \qquad 2.8$$

In the absence of leakage, the flux links the N turn winding N times. The flux linkage is

$$\lambda = N \phi \qquad 2.9$$

$$= \frac{2 \mu_0 N^2 I a b d}{X (2a + b)} \qquad 2.10$$

$$= L(X) I \qquad 2.11$$

$$L(X) = \frac{2 \mu_0 N^2 a b d}{X (2a + b)} \qquad 2.12$$

2.1.2 Experimentally Measured Inductance

The transducer exciter has a primary winding of 500 turns and a secondary winding of 26 turns on the center leg. A comparison is to be made between the theoretical transducer inductance and the measured primary and secondary inductances. Because the secondary inductance winding has only 26 turns, it must be normalized in proportion to the turns ratio squared if it is to be made comparable to the primary inductance on the same plot of inductance versus gap width.

$$L(X)_{s \text{ normalized}} = \left(\frac{500}{26} \right)^2 L(X)_{s \text{ measured}} \qquad 2.13a$$

$$= 370 \, L(X)_{sm} \qquad 2.13b$$

The theoretical transducer inductance is evaluated from equation 2.12 by substituting the transducer parameters from Figure 1.3.

$$L(X)_t = \frac{1.34 \times 10^{-4}}{X} \qquad 2.14$$

Plots of transducer inductances versus gap width are shown in Figures 2.3 and 2.4. Further comparative insight can be gained by taking the natural logarithm of equation 2.14 and differentiating with respect to ln X.

$$\ln L(X)_t = \ln 1.34 \times 10^{-4} - \ln X \qquad 2.15a$$

$$\frac{d \ln L(X)_t}{d \ln X} = -1 \qquad 2.15b$$

A logarithmic plot of theoretical transducer inductance versus gap width is a straight line with slope of minus one. Figure 2.5 shows logarithmic plots of theoretical, primary, and normalized secondary inductances.

The measured values of primary and secondary inductance vary considerably from the theoretical values. Inspection of Figure 2.11 shows that electric forces calculated using the theoretical transducer inductance are closer to the actual value of measured electric force than electric forces calculated using measured inductance values. The range of gap width for these calculations is from .003 to .004 meters. In the limiting cases of X = 0 and X = infinity, the measured inductance values are more accurate than theoretical ones. Theoretically, as X approaches infinity, the inductance approaches zero. And, as X approaches zero, the

GAP WIDTH	PRIMARY MEASURED INDUCTANCE	SECONDARY MEASURED INDUCTANCE	NORMALIZED SECONDARY INDUCTANCE	THEORETICAL INDUCTANCE
X	$L(X)_p$	$L(X)_{sm}$	$L(X)_{sn}$	$L(X)_t$
meters	henries	henries	henries	henries
0	.252	.00092	.340	∞
.00046	.144	.00055	.204	.291
.00173	.092	.00036	.133	.078
.00295	.076	.00029	.107	.0455
.00580	.061	.00023	.085	.023
.00915	.056	.00022	.081	.0146
∞	.050	.00019	.070	0

EXPERIMENTALLY MEASURED AND THEORETICAL TRANSDUCER INDUCTANCES

Figure 2.2

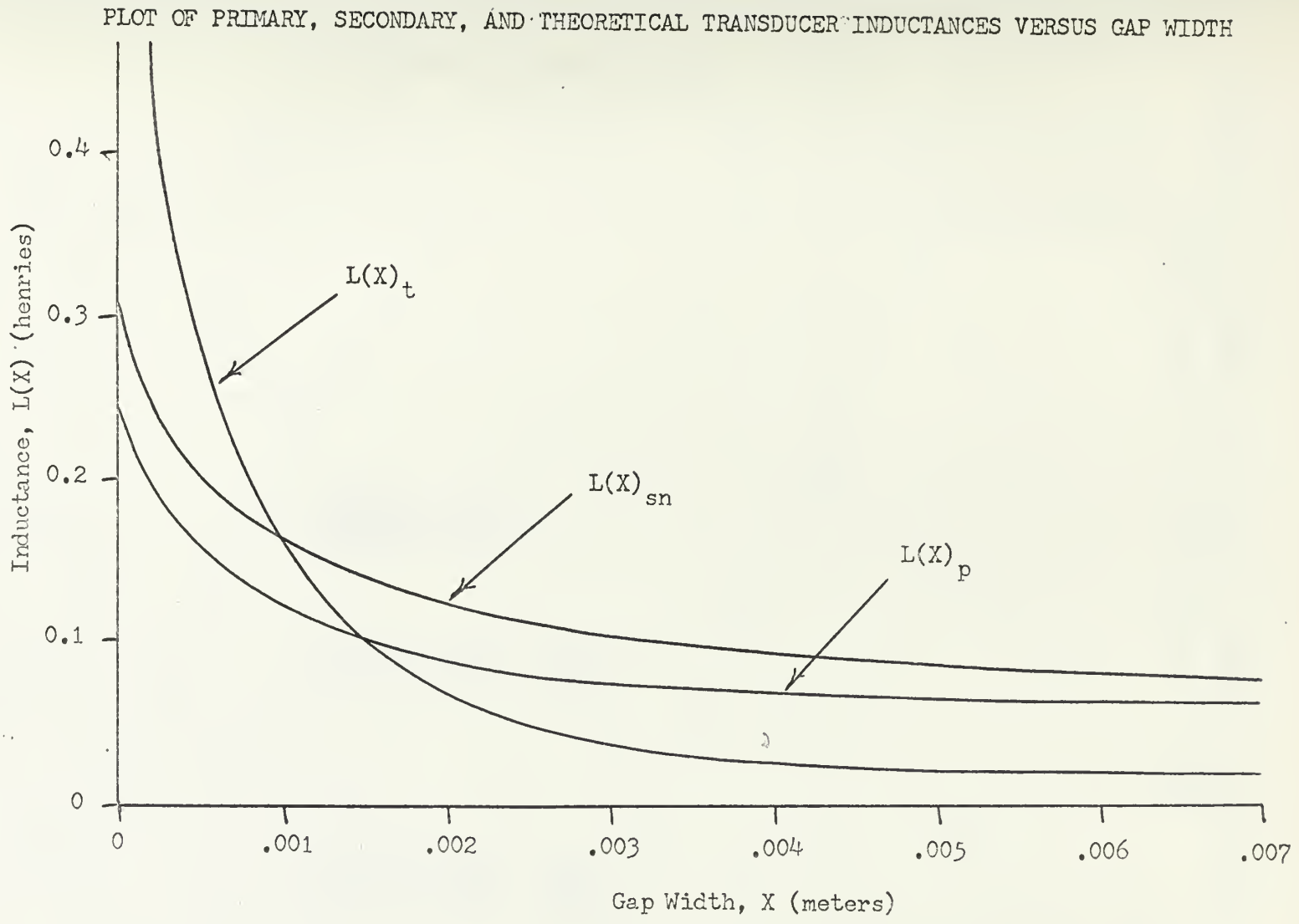
PLOT OF PRIMARY, SECONDARY, AND THEORETICAL TRANSDUCER INDUCTANCES VERSUS GAP WIDTH
Inductance, L(X) (henries)
0.4
0.3
0.2
0.1
0
$L(X)_t$
$L(X)_{sn}$
$L(X)_p$
0
.001
.002
.003
.004
.005
.006
.007
Gap Width, X (meters)

Figure 2.3

EXPANDED PLOT OF PRIMARY AND THEORETICAL TRANSDUCER INDUCTANCES VERSUS GAP WIDTH FOR DETERMINATION OF $\frac{dL(X)}{dX}$

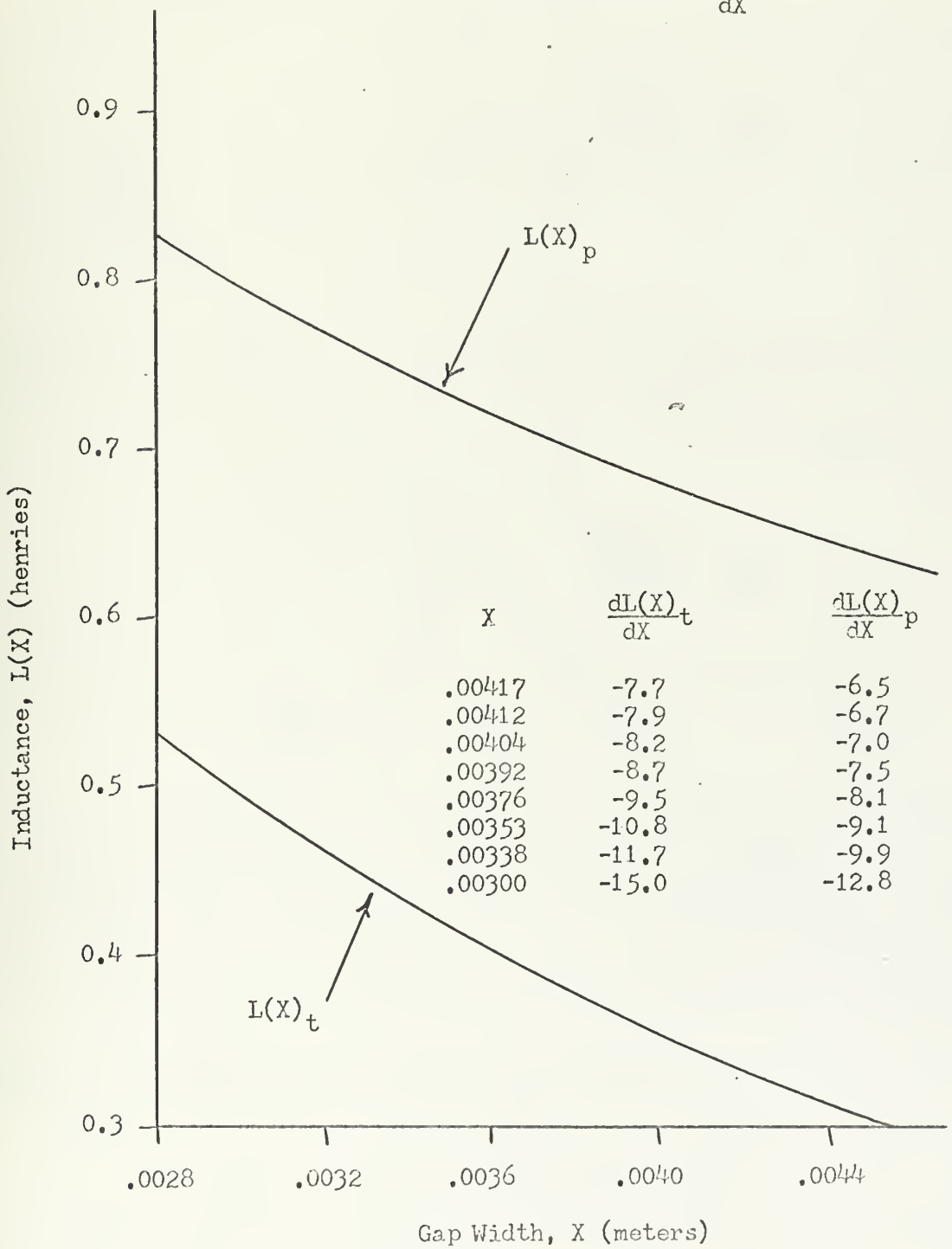

X	$\frac{dL(X)}{dX}_t$	$\frac{dL(X)}{dX}_p$
.00417	-7.7	-6.5
.00412	-7.9	-6.7
.00404	-8.2	-7.0
.00392	-8.7	-7.5
.00376	-9.5	-8.1
.00353	-10.8	-9.1
.00338	-11.7	-9.9
.00300	-15.0	-12.8

Figure 2.4

LOG-LOG PLOT OF PRIMARY, SECONDARY, AND THEORETICAL TRANSDUCER INDUCTANCES VERSUS GAP WIDTH

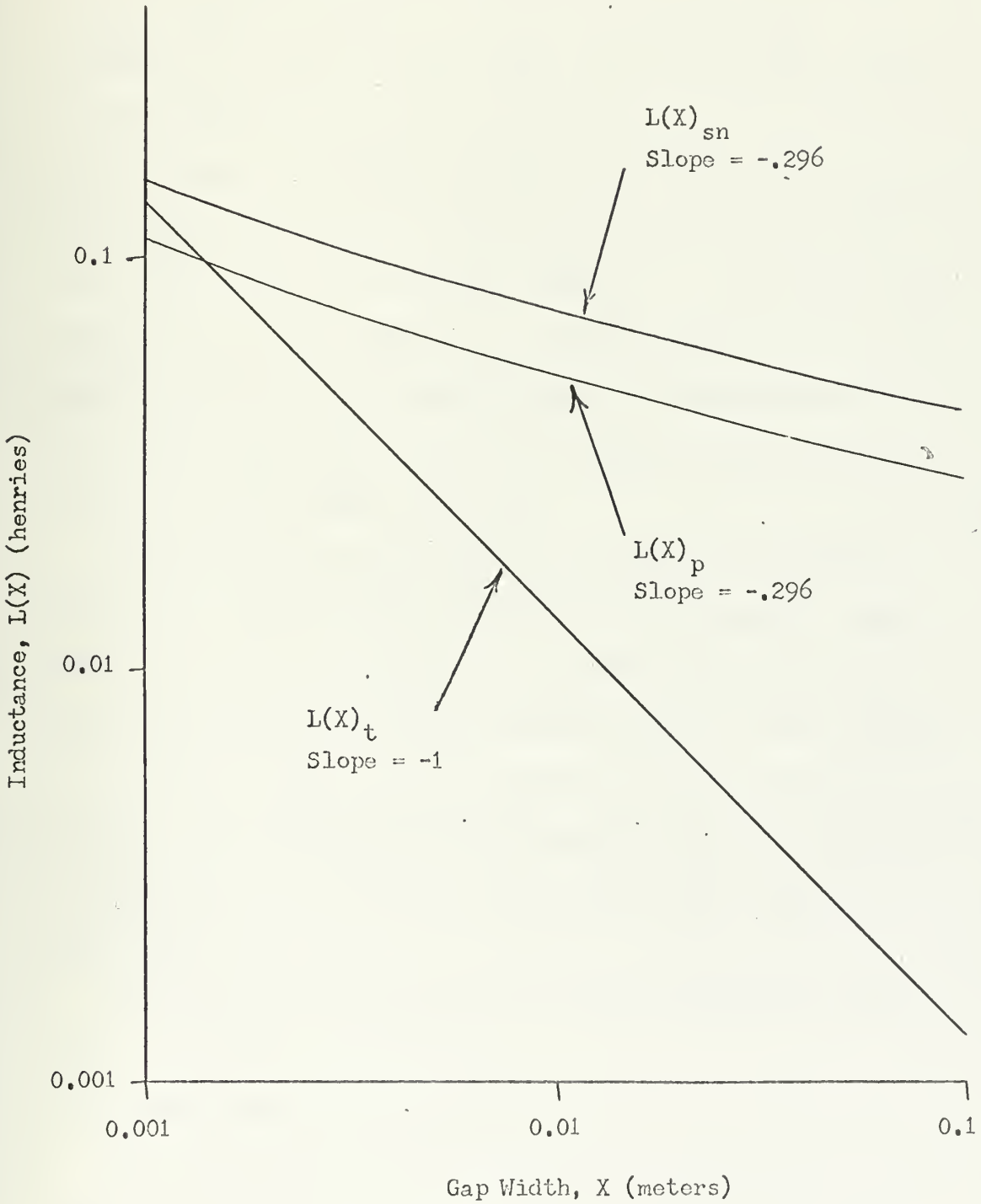

Figure 2.5

inductance becomes infinite. Practically, neither of these theoretical limits is accurate. In the real infinite limit, the gap width is so great that the magnetic field lines find a path of less reluctance by going directly from the center exciter leg to the outside legs through the air. Even in the case of less than infinite gap width, some field lines travel directly from leg to leg altering the transducer inductance. In the zero limit, when no air gap exists between the actuator and the exciter, the actual inductance is not infinite because the permeability of the actuator and exciter metal is not infinite, as was assumed in the theoretical model, but finite.

Fringing fields and non-infinite transducer permeabilities affect the measured inductance values for all gap widths. Field losses can account for the difference between primary and secondary inductances. The primary exciter winding is wound directly to the exciter center leg. The secondary winding is wound over the primary. The tendency would be for greater losses to be experienced in the secondary, resulting in a larger inductance. Figure 2.3 shows this to be true.

Additional errors could have come from the impedamce bridge used for inductance measurements.

2.2 Actuator Support Spring Constant

Each transducer actuator is supported by four springs. The value of the spring constant, K, for these springs was desired. Weights were placed on top of each actuator. The resulting

M	Mg	X	X_0-X
Mass	Weight Acting On Springs	Gap Width	Spring Deflection
kg.	newtons	meters	meters
0	0	X_0 = .00501	0
.297	2.91	.00398	.00103
.397	3.89	.00368	.00133
.497	4.87	.00328	.00173
.586	5.75	.00298	.00203
.675	6.62	.00268	.00233

DATA FOR SPRING CONSTANT EVALUATION

Figure 2.6

PLOT OF SPRING FORCE ACTING ON THE TRANSDUCER ACTUATOR VERSUS SPRING COMPRESSION

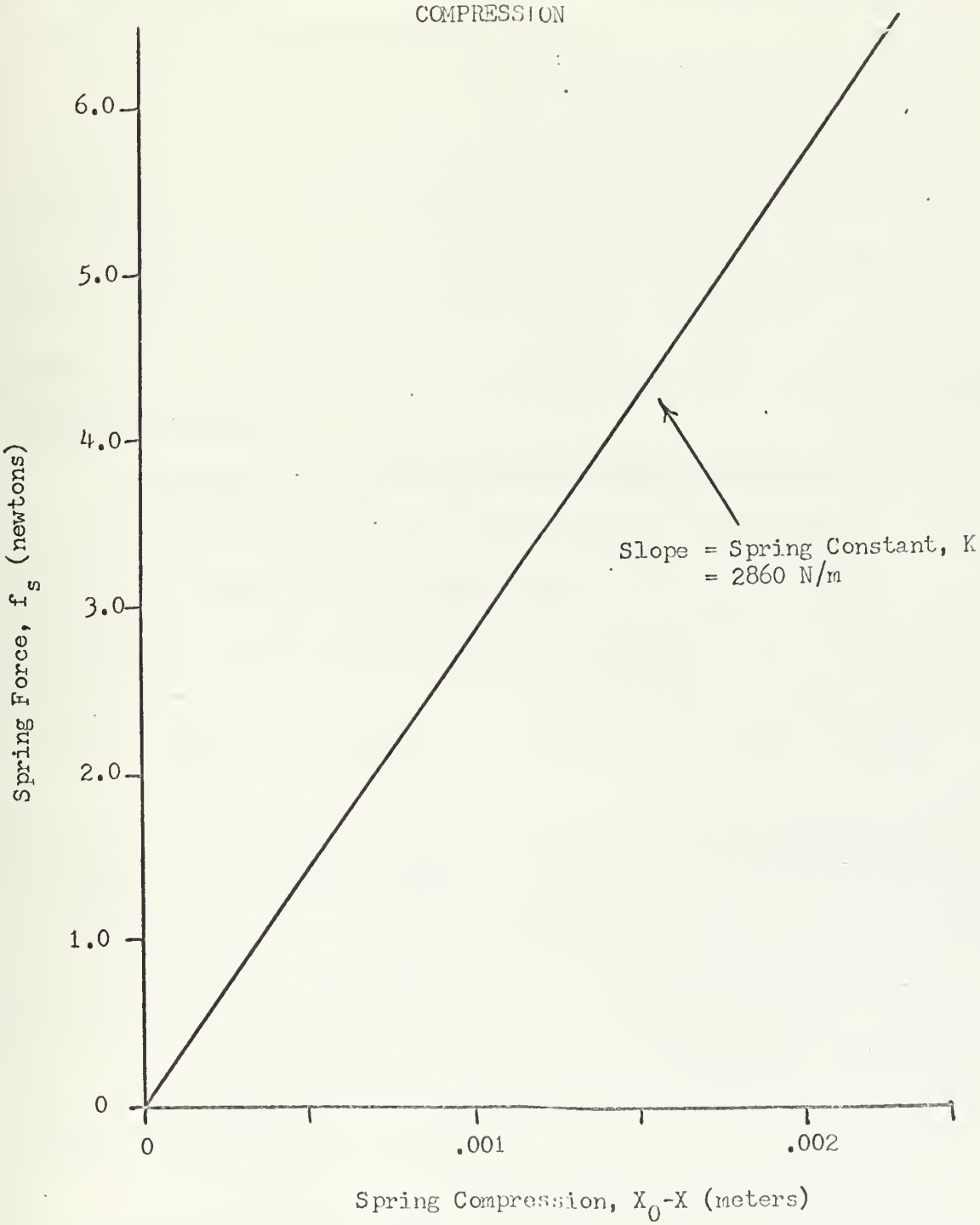

Figure 2.7

change in gap width due to these weights, which is the spring deflection, was measured with micrometers.

The values of weights and spring deflections are plotted on Figure 2.7. The spring constant for the four springs acting in parallel is the slope of the curve. Thus, the spring force, f_s, is expressed as $K (X_0 - X)$ where X_0 is the undeflected gap width. Figure 2.7 shows the spring constant to be 2860 newtons/meter.

2.3 Electric Forces

2.3.1 Electric Force Determination Using Energy Methods[10]

The magnetic transducer is represented as a two terminal circuit in Figure 2.8a. The total energy stored in the system is W_m. The power or rate of change of energy is

$$\frac{d W_m}{dt} = iv - f_e \frac{dx}{dt} \qquad 2.16$$

$$= i \frac{d\lambda}{dt} - f_e \frac{dx}{dt} \qquad 2.17$$

$$d W_m = i \, d\lambda - f_e \, dx \qquad 2.18$$

It is desired to have current as the variable, so a co-energy is defined as

$$d W'_m = -d W_m + i \lambda \qquad 2.19$$

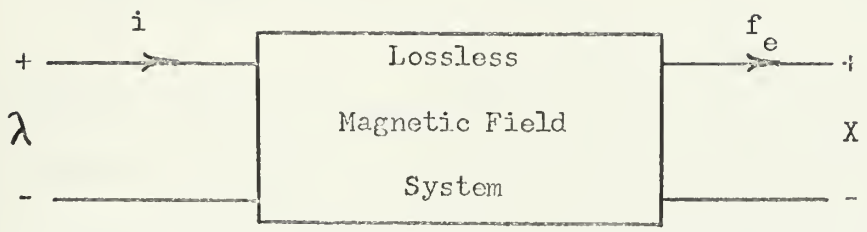

a. Terminal Pair Representation Of The Magnetic Transducer Circuit

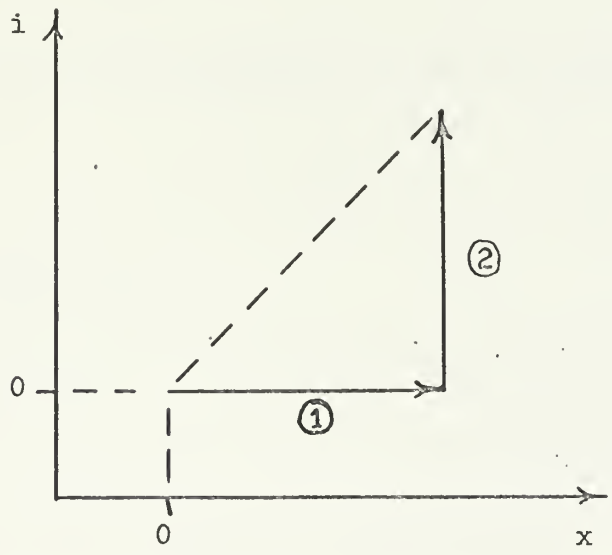

b. Paths Of Integration For Evaluation Of Magnetic Transducer Co-energy

Figure 2.8

Substitute equation 2.19 in 2.18.

$$d W'_m = \lambda di + f_e dx \qquad 2.20$$

Integrate the co-energy along the path shown in Figure 2.8b. The integral is independent of the path taken. Along path (1), current is zero so the electric force is zero. Along path (2), the displacement is at its final value, X.

$$W'_m = \int_{\substack{i=0}}^{X} f_e \, dx + \int_{\substack{x=X}}^{i} \lambda \, di \qquad 2.21$$

Using the value of λ from equation 2.10 and the definition of L(X) from 2.12,

$$W'_m = \frac{\mu_0 N^2 a b d}{X (2a + b)} I^2 \qquad 2.22$$

$$= \tfrac{1}{2} L(X) I^2 \qquad 2.23$$

In differential form, $d W'_m$ can be represented as

$$d W'_m = \frac{d W'_m}{di} di + \frac{d W'_m}{dx} dx \qquad 2.24$$

Compare this equation with equation 2.20.

$$\lambda = \frac{d W'_m}{di} \qquad 2.25$$

$$f_e = \frac{d\, W'_m}{dx} \qquad 2.26$$

From equation 2.22, the electric force is

$$f_e = -\frac{\mu_o N^2\, a\, b\, d}{X^2\,(2a + b)}\, I^2 \qquad 2.27$$

$$= \tfrac{1}{2}\frac{d\, L(X)}{dX}\, I^2 \qquad 2.28$$

2.3.2 Electric Force Determination Using Maxwell Stress Tensor[11]

The electric force on the transducer actuator in the x direction is desired. This is evaluated using the definition of the stress tensor in Figure 2.9. Since the only magnetic fields are in the x direction, only an x component of the stress tensor exists.

$$T_{xx} = \tfrac{1}{2}\mu_0 \left(H_1^2 + H_2^2 + H_1^2 \right) \qquad 2.29$$

$$f_e = \int_S T_{xx} \cdot n\, da \qquad 2.30$$

$$= \tfrac{1}{2}\mu_0 \left(2\, H_1^2\, a\, d + H_2^2\, b\, d \right) \qquad 2.31$$

Substitute equations 2.5 and 2.6 for H_1 and H_2.

$$f_e = \frac{\mu_0 N^2\, a\, b\, d}{X^2\,(2a + b)}\, I^2 \qquad 2.32$$

which is identical to equation 2.27.

MAXWELL STRESS TENSOR REPRESENTATION OF THE TRANSDUCER ACTUATOR ELECTRIC FORCE

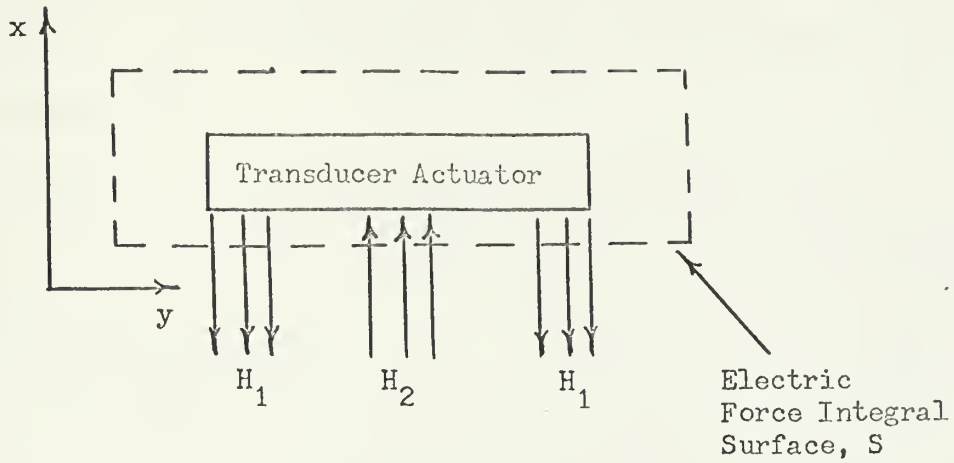

$$T_{mn} = \mu H_n H_m - \tfrac{1}{2}\mu \delta_{mn} H_k H_k$$

$$\delta_{mn} = 1 \text{ if } m=n$$

$$= 0 \text{ if } m \neq n$$

Figure 2.9

2.3.3 Experimental Evaluation Of Electric Force

For any applied current to the exciter windings, the actuator will assume an equilibrium position such that the springs are compressed and exert an upward spring force which is balanced by the applied electric force and the weight of the actuator acting downward.[12]

The actuator weight is balanced by an equilibrium spring force.

$$Mg = K (X_0 - X_1) \qquad 2.33$$

The electric force will then be balanced by the additional compression of the springs.

$$f_{em1} = K (X_1 - X) \qquad 2.34$$

This force is the experimentally measured electric force.

The electric force can be determined in two other ways. Theoretically it is

$$f_{et1} = \tfrac{1}{2} \frac{d\, L(X)_t}{dX} \Big|_X I^2 \qquad 2.35$$

from equation 2.28 where $\frac{d\, L(X)}{dX}$-t is the slope of Figure 2.4.

By use of measured inductances and the slope of the measured inductance curve, measured electric forces are

I	X	$X_1 - X$	f_{em1}	$\frac{dL(X)}{dX}_t$	f_{et1}	$\frac{dL(X)}{dX}_p$	f_{em2}
Transducer Current	Gap Width	Spring Comp.	Meased. Spring Force		Theoret. Elect. Force		Meased. Elect. Force
Amps.	meters	meters	newtons	h/m	newtons	h/m	newtons
0	X_1 =.00417	0	0	-7.7	0	-6.5	0
0.1	.00417	0	0	-7.7	-.038	-6.5	-.032
0.2	.00412	.00005	..143	-7.9	-.158	-6.7	-.134
0.3	.00404	.00013	.372	-8.2	-.369	-7.0	-.312
0.4	.00392	.00025	.715	-8.7	-.697	-7.5	-.590
0.5	.00376	.00041	1.170	-9.5	-1.19	-8.1	-1.010
0.552	.00353	.00064	1.830	-10.75	-1.65	-9.1	-1.400
0.604	.00338	.00079	2.260	-11.7	-2.13	-9.9	-1.810
0.656	.00300	.00117	3.340	-15.0	-3.23	-12.8	-2.750
0.677	0	.00417	Closed Off				

DATA FOR PLOTS OF ELECTRIC FORCE

Figure 2.10

PLOT OF SPRING, THEORETICAL ELECTRIC, AND MEASURED ELECTRIC FORCES VERSUS GAP WIDTH

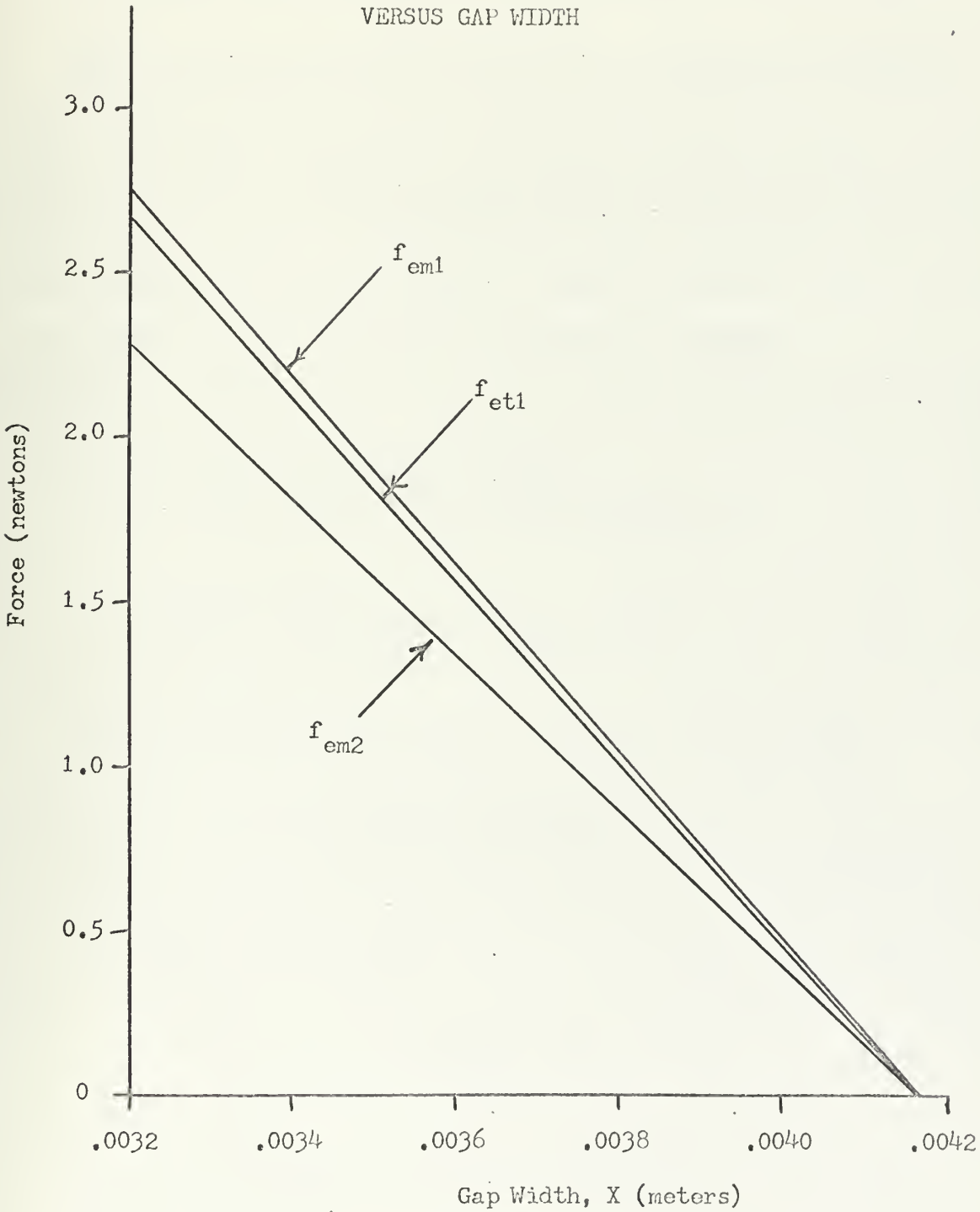

Figure 2.11

$$f_{em2} = \tfrac{1}{2} \left. \frac{d\, L(X)_p}{dX} \right|_X I^2 \qquad 2.36$$

Over the range of gap widths measured, the theoretical electric force most accurately predicts the actual electric force, f_{em1}. The electric force calculated from the measured inductance is considerably in error. It was evaluated using the slope of the measured inductance curve, Figure 2.4, from section 2.1.2. An error might have been expected for the reasons previously mentioned in section 2.1.2.

2.4 Magnetic Transducer Force Equilibrium

Newton's law applied to the transducer actuator is

$$M \frac{d^2x}{dt^2} + D \frac{dx}{dt} = f_{spring} + f_{electric} - Mg \qquad 2.37$$

The position that the transducer actuator takes in steady state equilibrium represents a balance between the upward spring force and the downward electric and weight forces.(13)

$$F(X) = f_s + f_e - Mg \qquad 2.38$$

$$= K (X_0 - X) + \frac{\mu_0 N^2 a b d}{X^2 (2a + b)} I^2 - Mg \qquad 2.39$$

$$= K (X_0 - X_1) + K (X_1 - X) + \frac{\mu_0 N^2 abd}{X^2 (2a+b)} I^2 - Mg \qquad 2.40$$

The weight of the actuator cancels $K (X_0 - X_1)$.

$$F(X) = K\,(X_1 - X) + \frac{\mu_0 N^2 \text{ abd } I^2}{X^2\,(2a + b)} \qquad 2.41$$

Figure 2.13 is a plot of these two functions of X. The points where they intersect are the equilibrium operating points or the equilibrium positions assumed by the actuator. A separate plot will be obtained for any value of current. The points, X_u, are unstable equilibrium points. A change in X from this value causes a force imbalance which tends to cause X to change even further. The points, X_s, are stable. Any change in X from X_s causes a force imbalance which tends to return the actuator back to X_s. The actuator always takes a stable position.

As current is increased beyond 0.677 amperes, the values of electric force are always greater than spring force. There are no equilibrium positions for the actuator. Electric force always overcomes the springs and closes off the gap. The point of tangency, X_T, is the equilibrium position for the actuator when current is equal to 0.677 amperes. Any perturbation acting to increase X causes the actuator to return to X_T. But, any perturbation which acts to decrease X will cause the actuator to close off to X = 0.

The accuracy of Figure 2.13 can be checked. Each stable equilibrium point, X_s, on Figure 2.13 should correspond to the measured gap width from figure 2.10 for the same value of current. Examination shows this to be true.

I	$-f_e$	$X=1x10^{-3}$	$X=2x10^{-3}$	$X=3x10^{-3}$	$X=4x10^{-3}$	$X=5x10^{-3}$
Exciter Current	Elect. Force					
Amp.	Newtons					
0.2	$f_{e0.2}$	2.68	0.67	0.30	0.17	0.11
0.4	$f_{e0.4}$	10.7	2.67	1.20	0.67	0.43
0.552	$f_{e0.552}$	20.5	5.10	2.29	1.27	0.82
0.656	$f_{e0.656}$	28.9	7.20	3.23	1.81	1.20
0.677	$f_{e0.677}$	30.7	7.65	3.44	1.93	1.24

DATA FOR PLOTS OF ELECTRIC FORCE VERSUS

GAP WIDTH

Figure 2.12

PLOT OF SPRING AND ELECTRIC FORCES VERSUS GAP WIDTH FOR VARIOUS CURRENTS

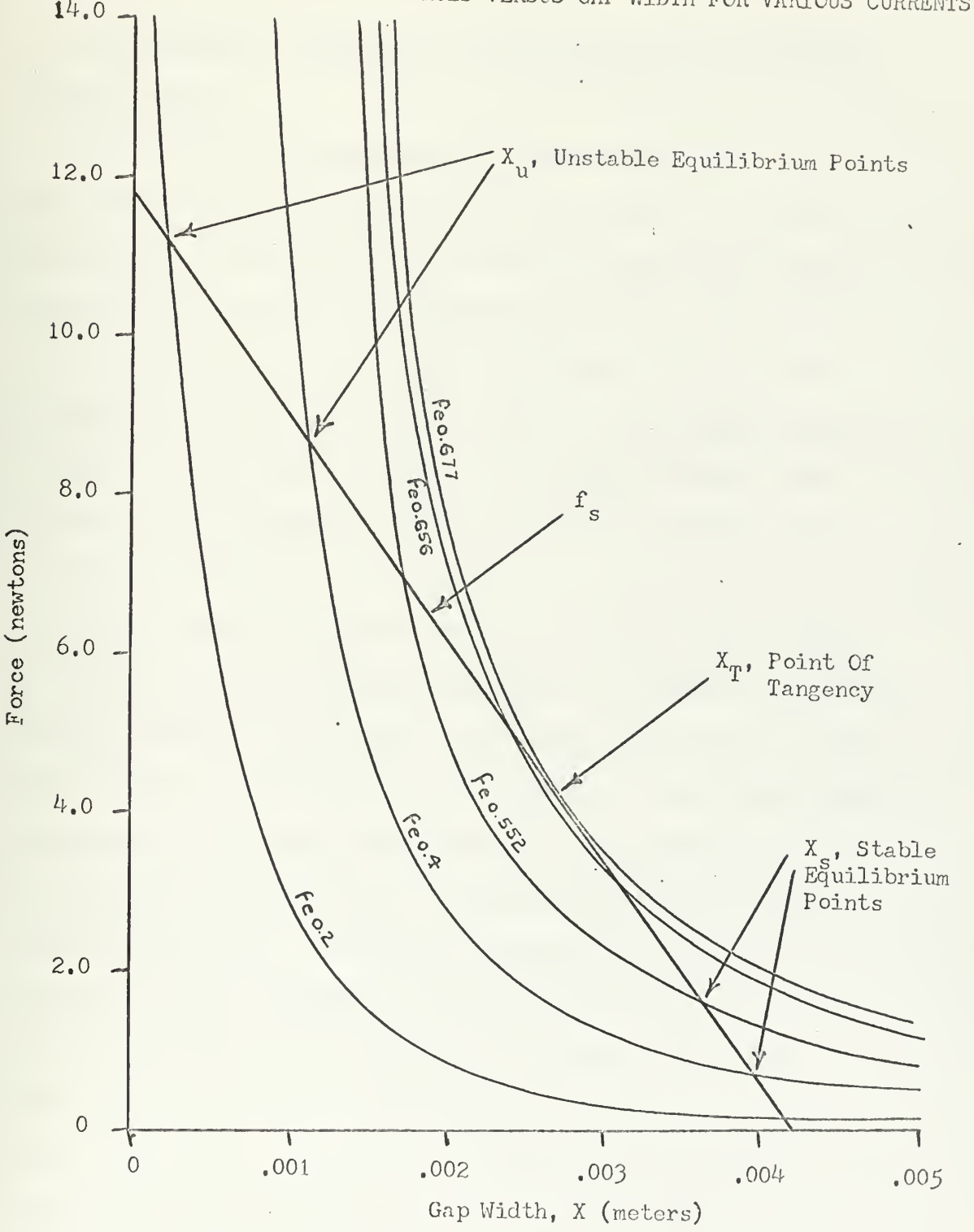

Figure 2.13

2.5 Time Variation Of Transducer Actuator Position For Sinusoidal Applied Current

Plots of actuator position versus time are obtained using the current-gap width correspondence from Figure 2.10. Figures 2.14a, 2.15a, 2.16a, and 2.17a are plots of time varying applied current and time varying head position for various combinations of direct bias current and alternating current. The gap width "closes off" at X = .00173 meters because the tube support spacer, as shown in Figure 1.2c, prevents it from going to zero. When the pump tube is inserted, it will be squeezed completely shut in this condition.

It was desired to operate the pump less than fully occluded. In concept this could have been accomplished by limiting the exciter currents such that the actuator never fully closed off the channel. Such operation is illustrated in Figure 2.17a. Under these conditions, the channel has a steady state width and a time variation in width around the steady state. Schematically this is shown in Figure 1.1 when $R > r$. Practically, operation of the pump as described is very difficult. During operation, variation in the characteristics of the individual transducers from each other cause one to operate properly while another closes off. Figure 2.17c shows actuator three operating almost properly, while the other three are closing off. The transducers are so unstable that only slight perturbations are necessary to make the gap close off completely.

To overcome this difficulty, a channel limiter was placed astride the pump tube. Actuator motion is restricted because the actuator contacts the rigid limiter as it tries to close off. The pump transducers can be driven as hard as desired, but peristalsis takes place only on that section of the tube above the limiter. The thickness of the limiter can be varied to obtain the desired values of R and r. Figure 2.16a illustrates the time variation of actuator motion with the limiter in place and Figure 2.16c shows the Sanborn recordings of actuator motion under these circumstances.

Figures 2.14b, 2.15b, 2.16b, and 2.17b are representations of the positions of the four actuators for various times covering one complete cycle. Each actuator is phased ninety degrees from the preceeding one. The result is a traveling wave to the right which can be approximated as a square wave or as sinusoidal.

Finally, Figures 2.14c, 2.15c, 2.16c, and 2.17c, two of which have already been discussed, are Sanborn recorder plots of actuator position versus time for all four transducer actuators. The plots are from the output of photo electric cells which were arranged to sense the motions of the actuators. Determination of the exact magnitudes of gap widths is not possible from the recordings because the recording amplitudes are relative and a function of the sensitivity setting. However, the recordings do illustrate the phase shift between the actuators which creates the traveling wave. The phase shift is not ninety degrees between

each actuator. The outputs of the power supplies for the exciter currents were not quite properly phased. The resulting traveling wave was uneven: close close pause close close pause close close.....

A comparison between the predicted actuator time varying position (e.g. Figure 2.15a) and one cycle of an actual measured time variation (e.g. Figure 2.15c) shows that the actual motion conforms quite well to predicted motion. The operation of the transducer is effectively open-closed. The transducer is so unstable that it acts almost like an on-off relay. This leads to the conclusion that an elaborate multi-phase sinusoidal power supply is not necessary for efficient operation of the pump. A simple on-off direct current power supply for each transducer which is actuated ninety degrees ahead of its predecessor is sufficient.

THEORETICAL TRANSDUCER EXCITER CURRENT AND ACTUATOR POSITION VERSUS TIME

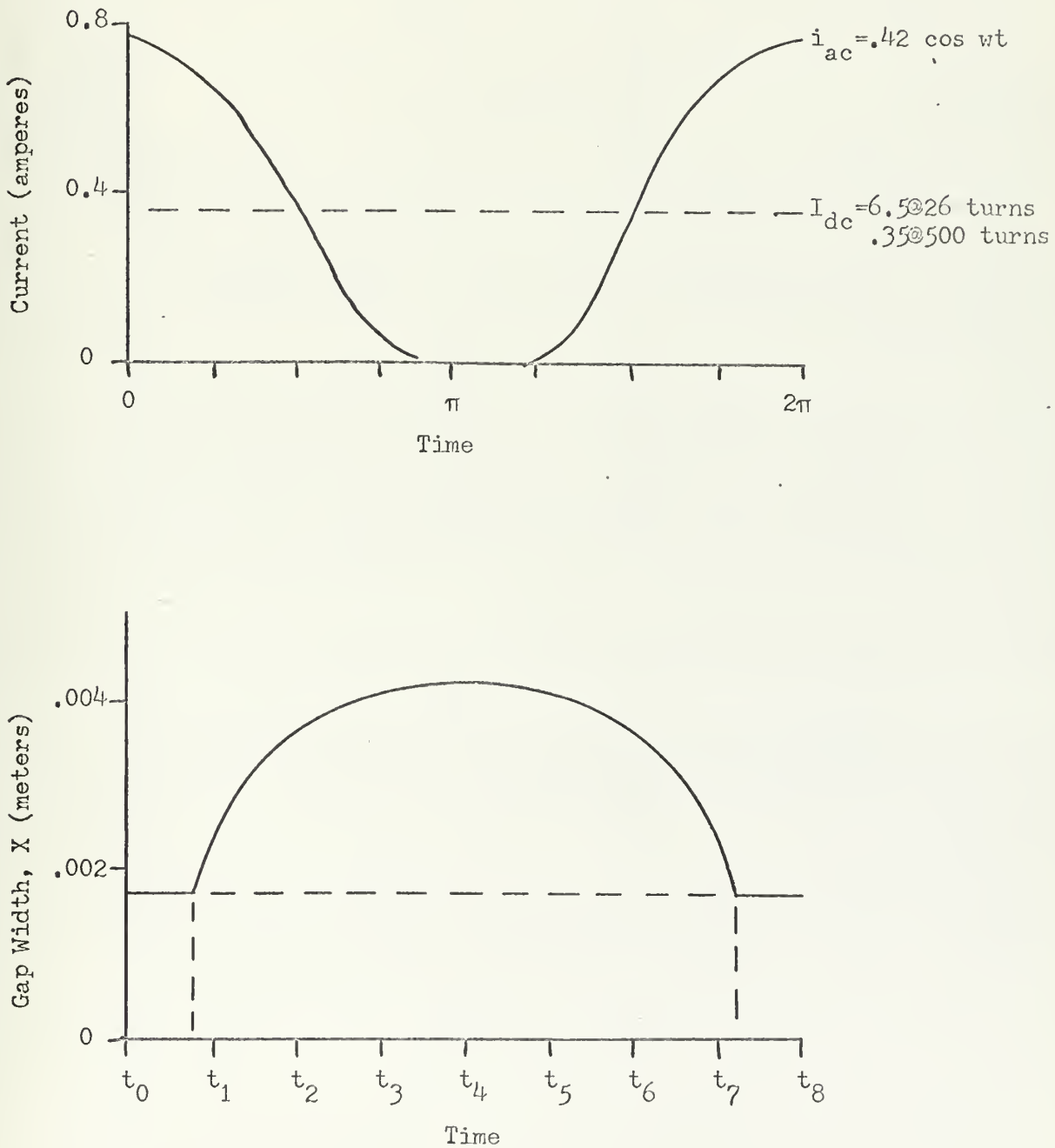

Figure 2.14a

THEORETICAL TRANSDUCER ACTUATOR POSITIONS FOR VARIOUS TIMES

PLOTS OF GAP WIDTH VERSUS ACTUATOR NR.

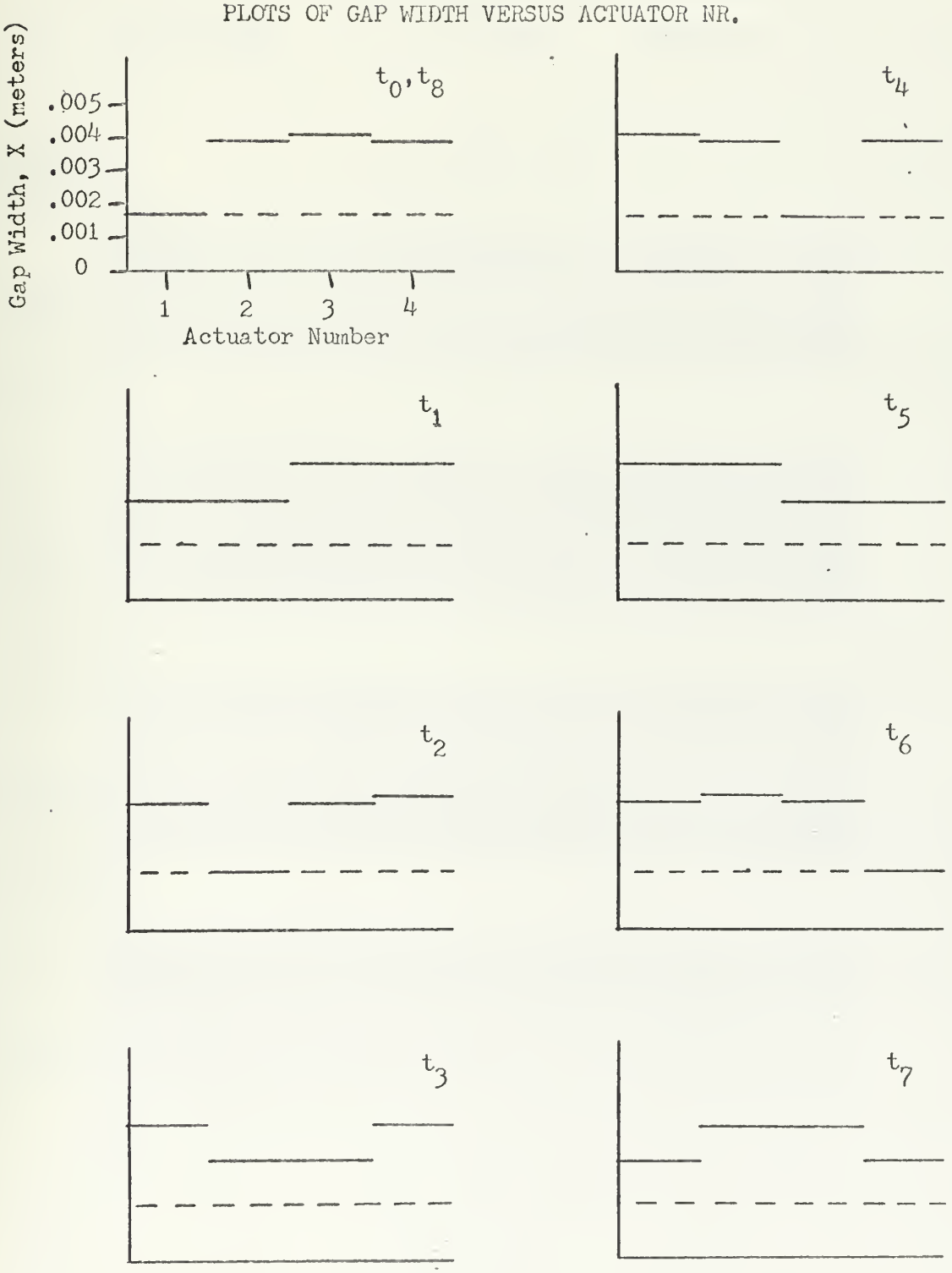

Figure 2.14b

SANBORN RECORDER PLOTS OF TRANSDUCER ACTUATOR MOTION VERSUS TIME

I_{dc} = 6.5 @ 26 turns
.35 @ 500 turns

i_{ac} = .42 cos wt

Frequency = 0.33

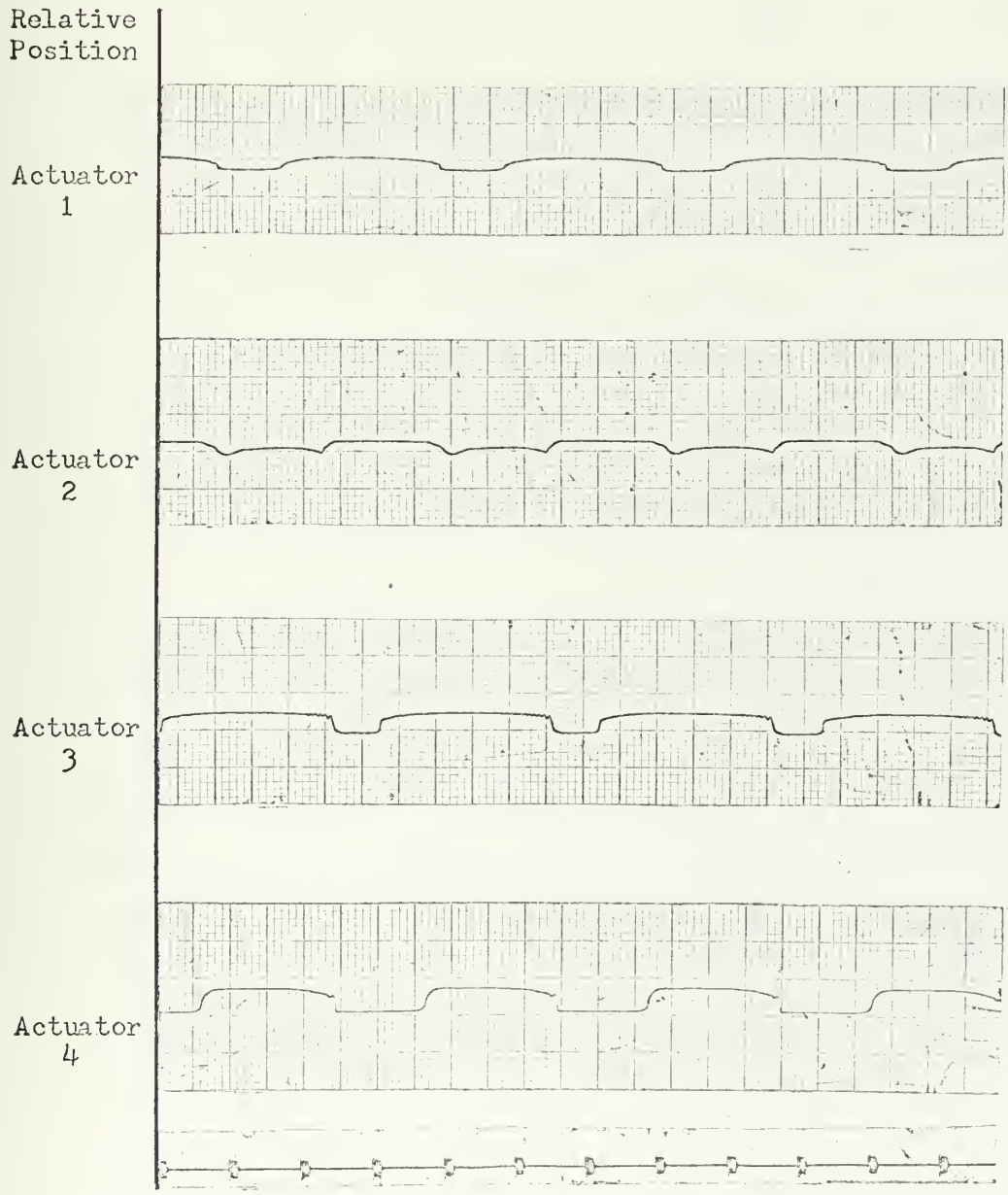

Figure 2.14c

THEORETICAL TRANSDUCER EXCITER CURRENT AND ACTUATOR POSITION

VERSUS TIME

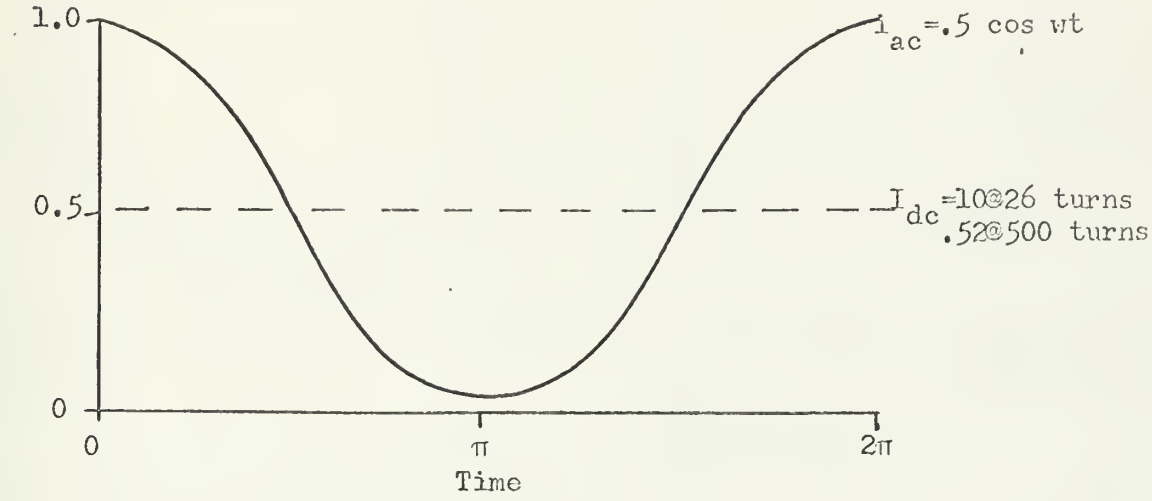

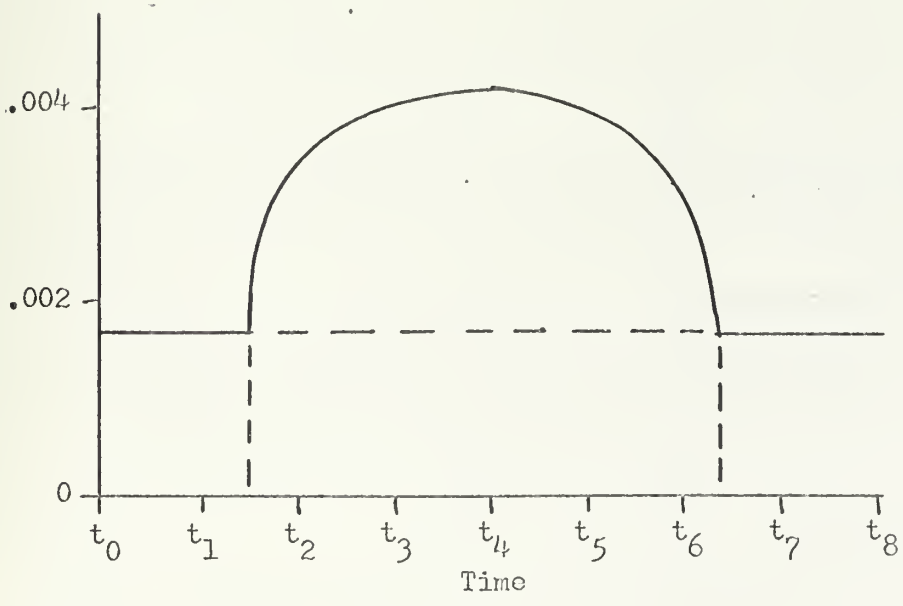

Figure 2.15a

THEORETICAL TRANSDUCER ACTUATOR POSITIONS FOR VARIOUS TIMES

PLOTS OF GAP WIDTH VERSUS ACTUATOR NUMBER

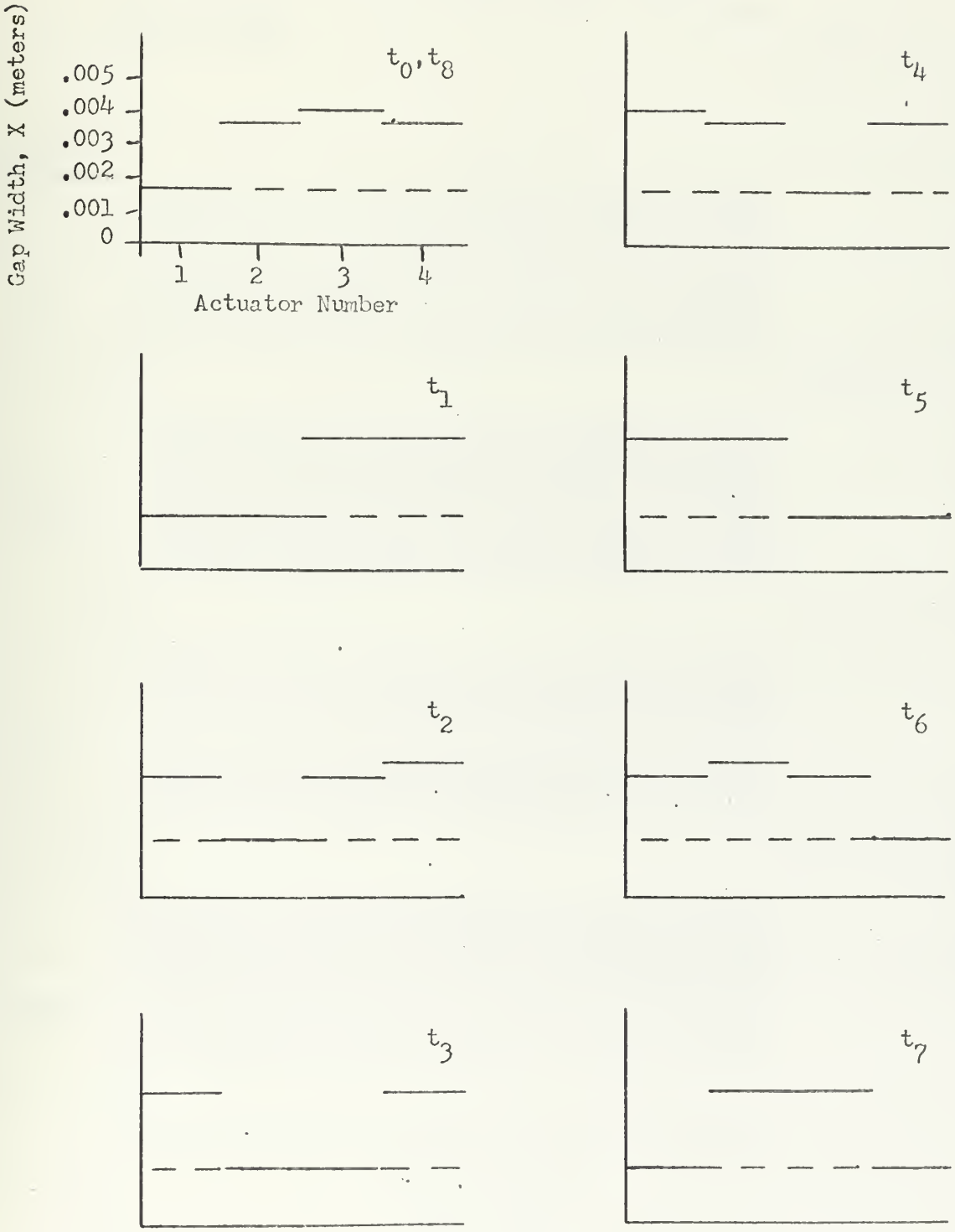

Figure 2.15b

SANBORN RECORDER PLOTS OF TRANSDUCER ACTUATOR MOTION VERSUS TIME

I_{dc} = 10 @ 26 turns
.52 @ 500 turns

i_{ac} = 0.5 cos wt

Frequency = 0.33

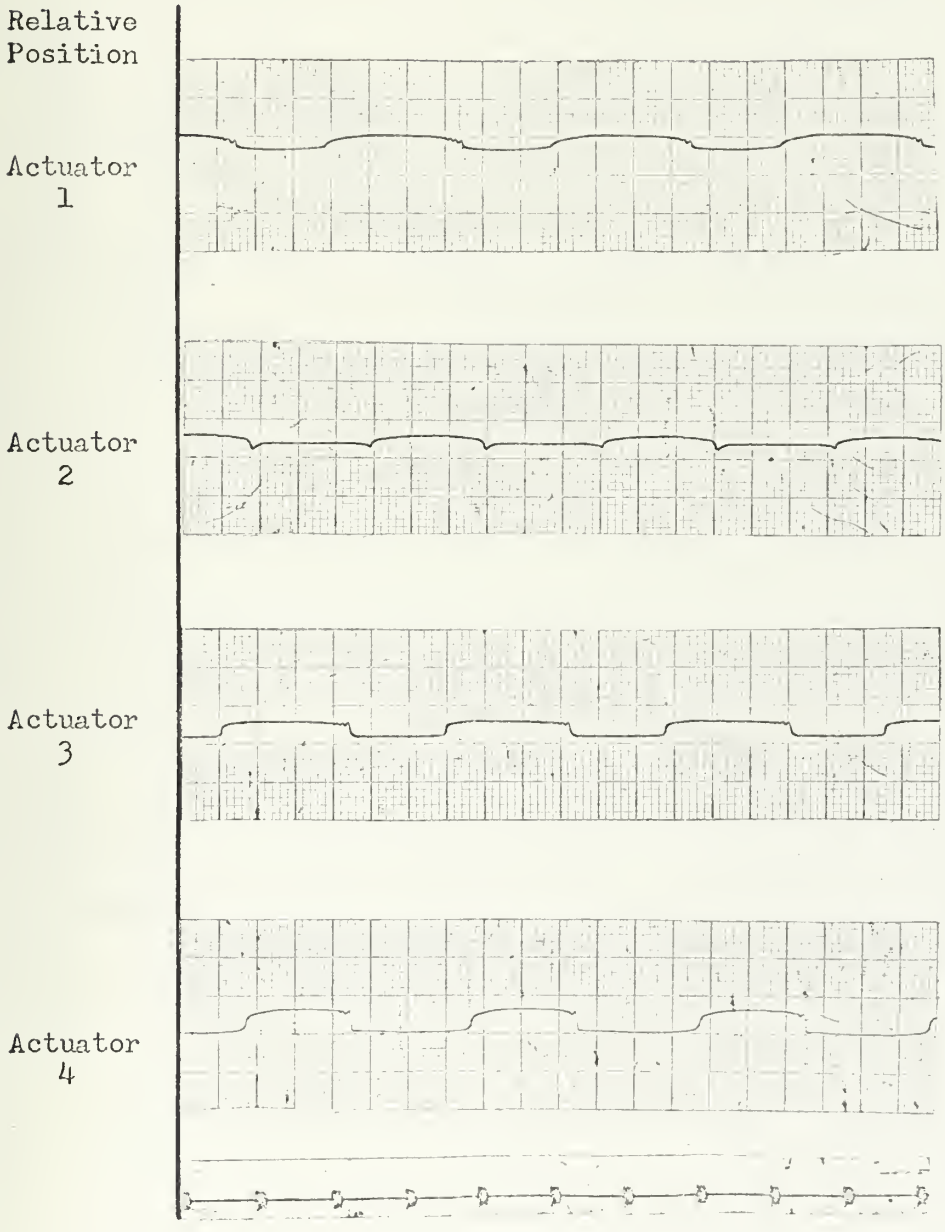

Figure 2.15c

THEORETICAL TRANSDUCER EXCITER CURRENT AND ACTUATOR POSITION VERSUS TIME

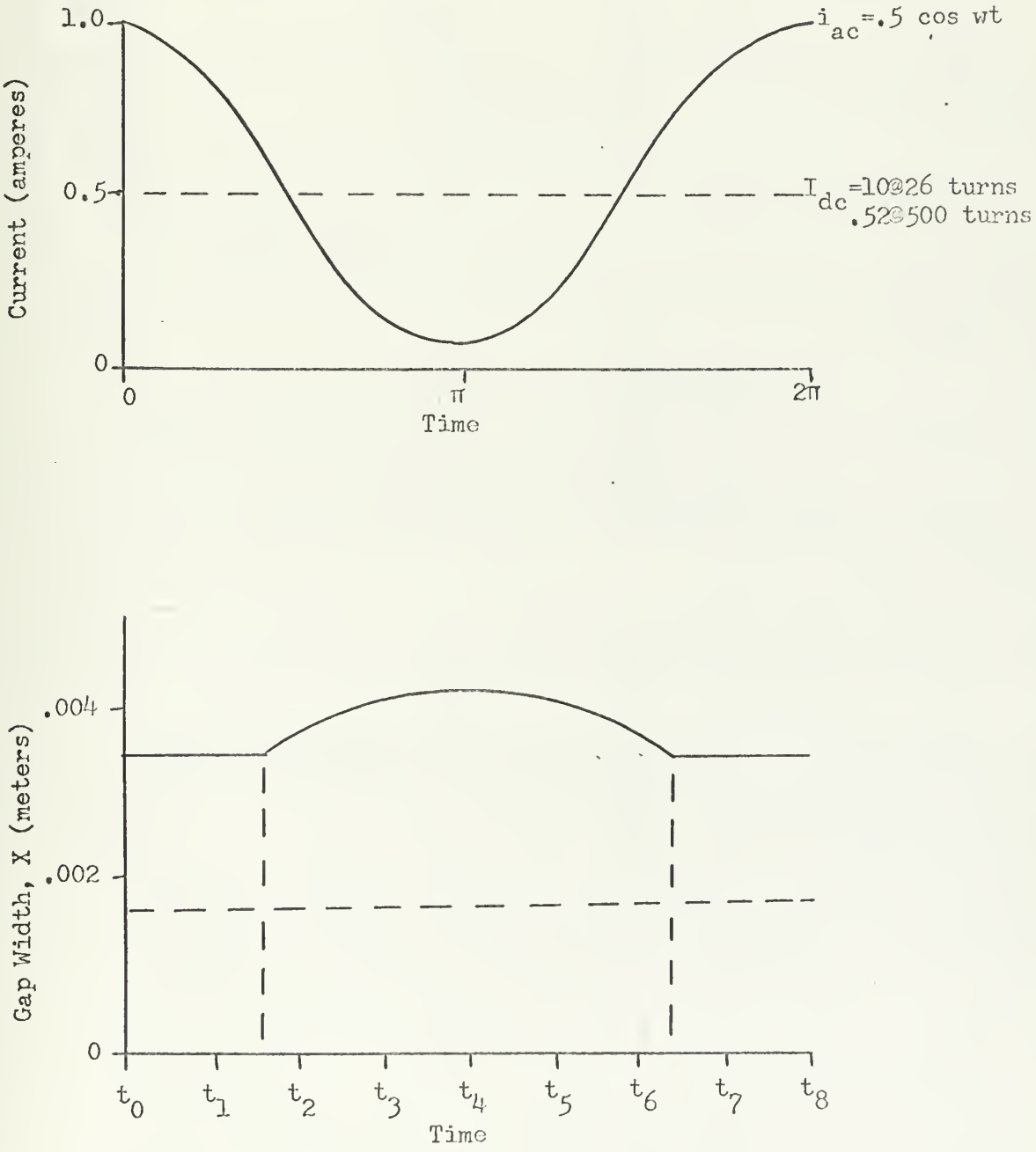

Figure 2.16a

THEORETICAL TRANSDUCER ACTUATOR POSITIONS FOR VARIOUS TIMES

PLOTS OF GAP WIDTH VERSUS ACTUATOR NUMBER

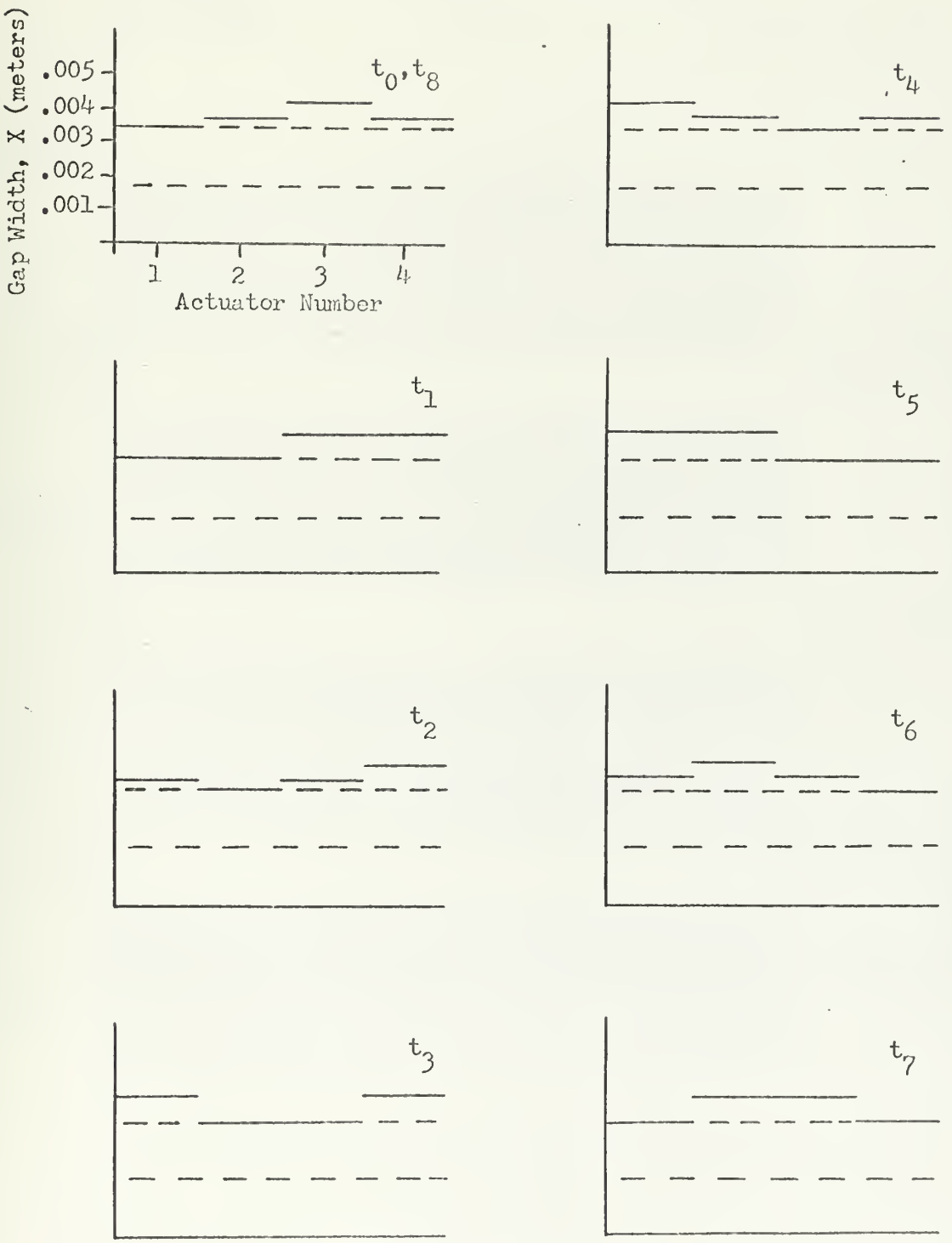

Figure 2.16b

SANBORN RECORDER PLOTS OF TRANSDUCER ACTUATOR MOTION VERSUS TIME

I_{dc} = 10 @ 26 turns
.52 @ 500 turns

i_{ac} = 0.5 cos wt

Frequency = 0.33

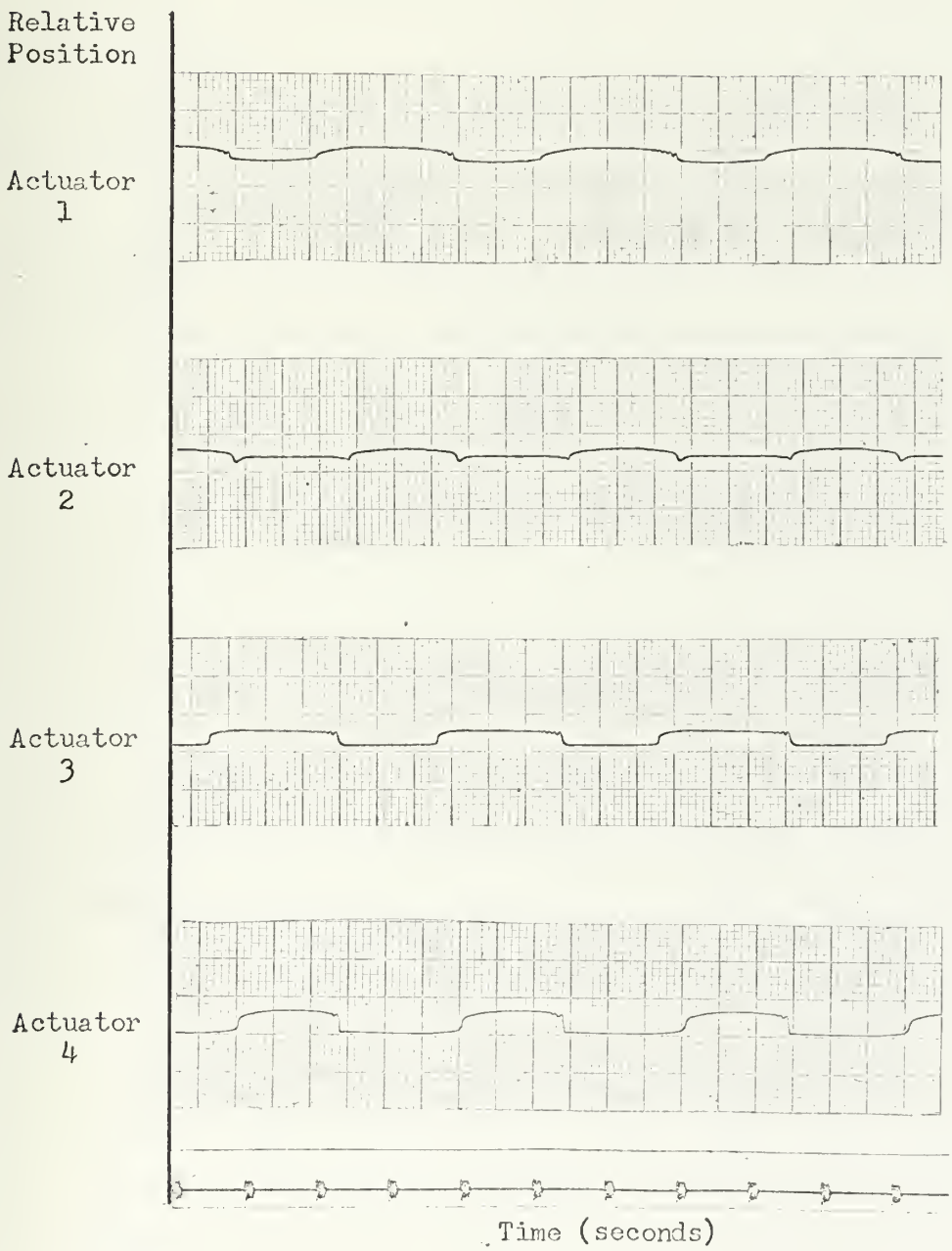

Figure 2.16c

THEORETICAL TRANSDUCER EXCITER CURRENT AND ACTUATOR POSITION VERSUS TIME

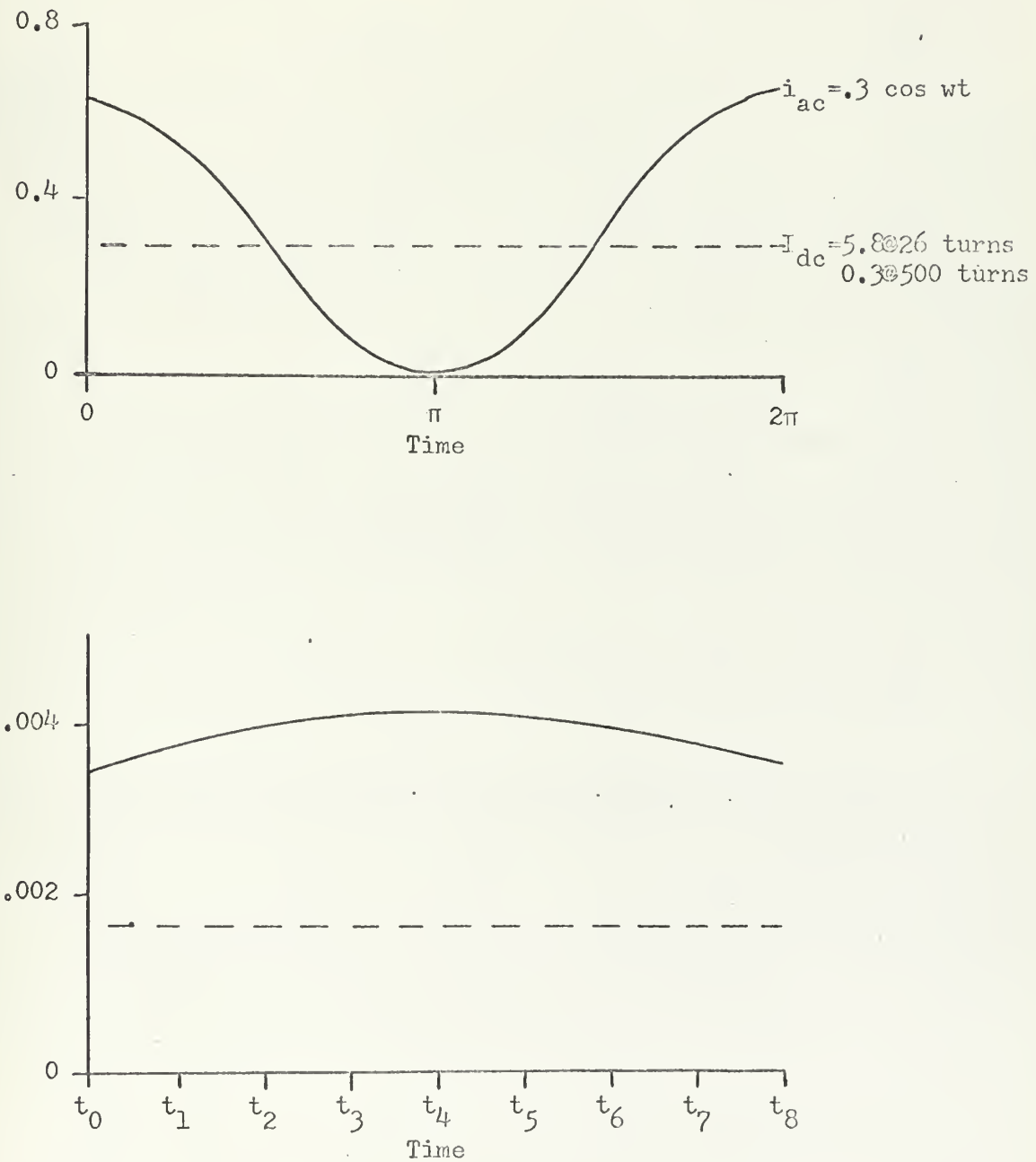

Figure 2.17a

THEORETICAL TRANSDUCER ACTUATOR POSITIONS FOR VARIOUS TIMES

PLOTS OF GAP WIDTH VERSUS ACTUATOR NUMBER

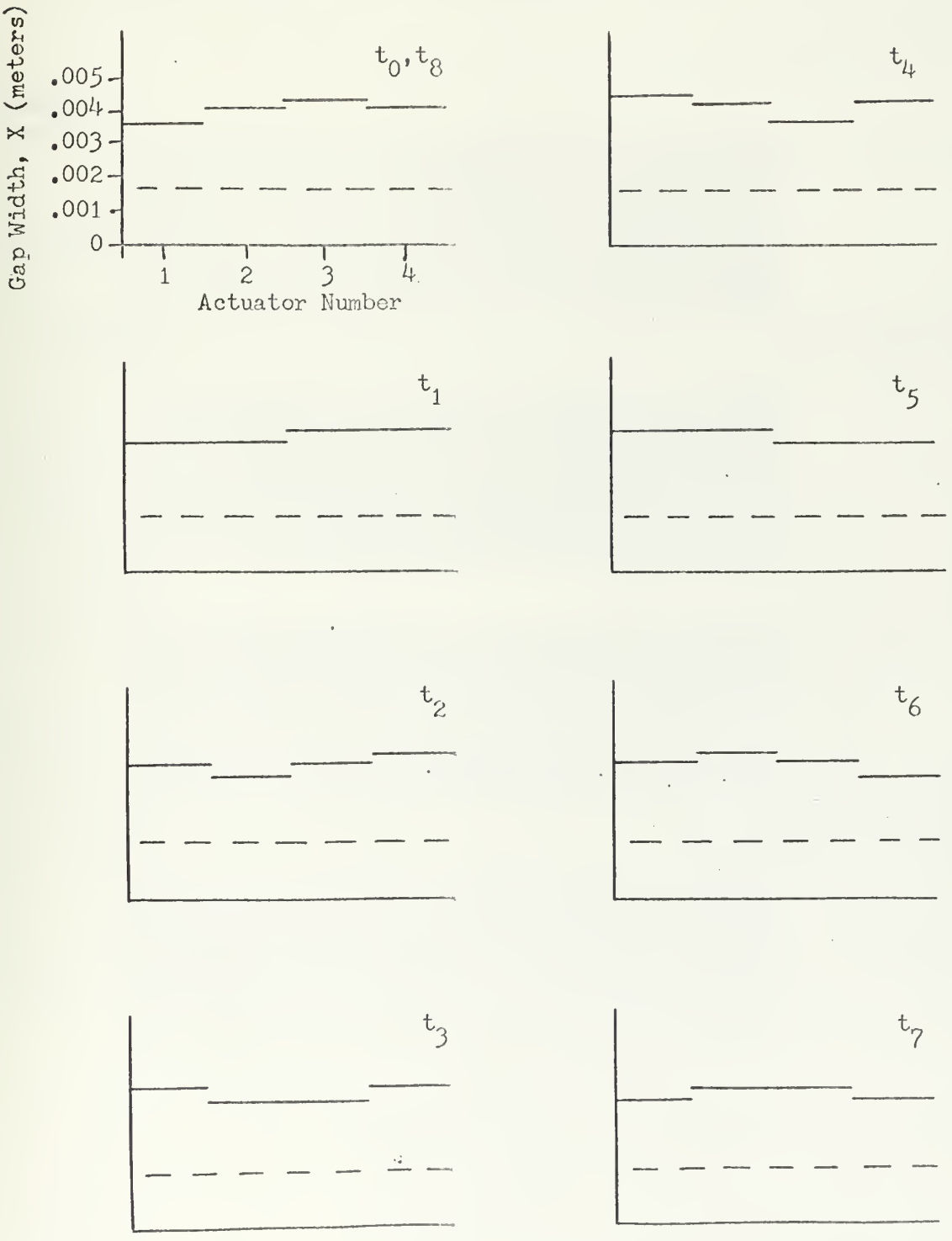

Figure 2.17b

SANBORN RECORDER PLOTS OF TRANSDUCER ACTUATOR MOTION VERSUS TIME

I_{dc} = 5.8 @ 26 turns
0.3 @ 500 turns

i_{ac} = .30 cos wt

Frequency = 0.33

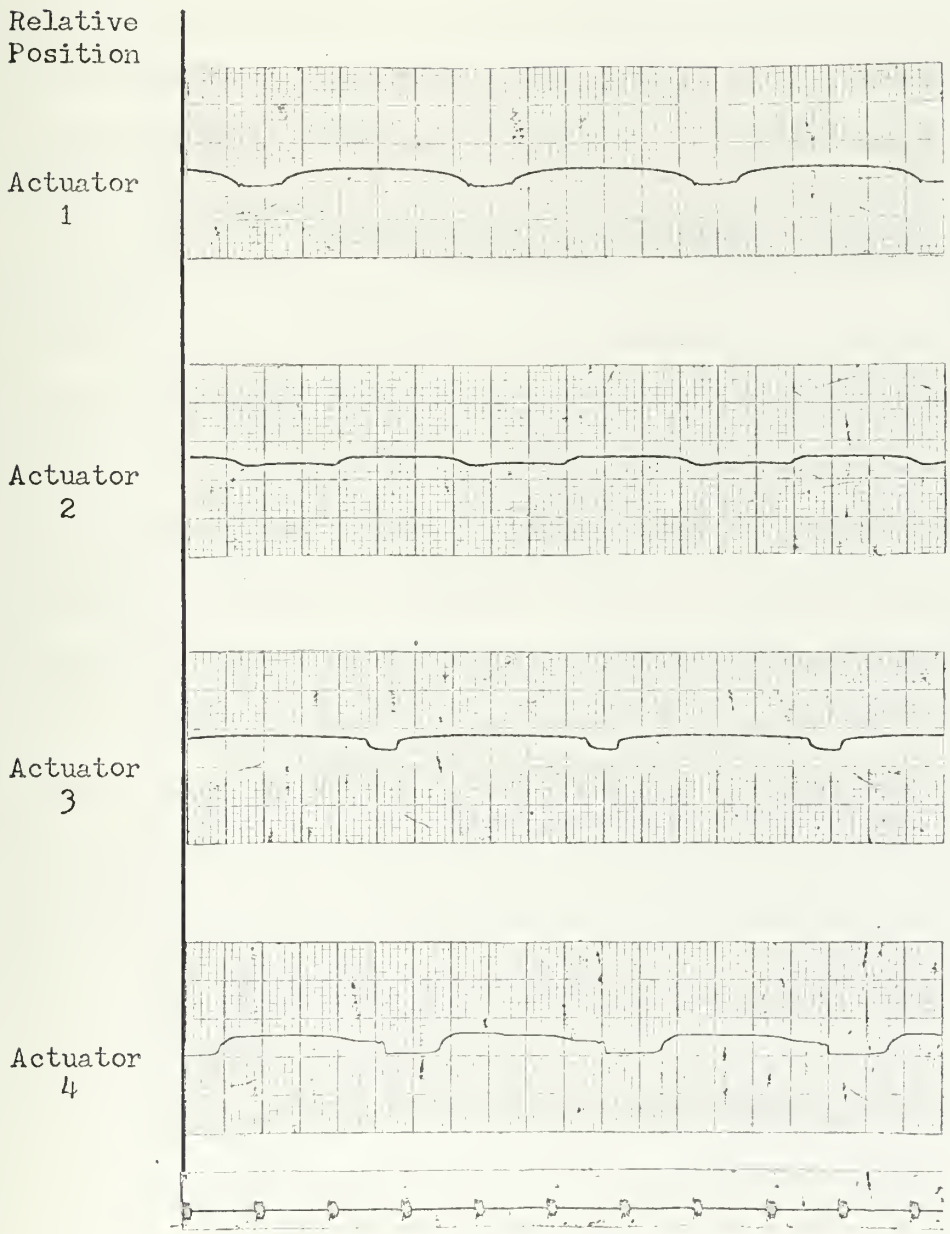

Figure 2.17c

CHAPTER III

PERISTALTIC PUMP ANALYSIS

Analysis of the electrical and mechanical properties of individual transducers has been completed in the previous chapter. This chapter is concerned with the analysis of the peristaltic pump as a whole. The fluid filled tube running between each transducer actuator and exciter exerts an upward pressure force on the actuator that must be determined and entered into the force balance on the actuator. The magnitude of this upward pressure force relative to the electric force, which acts to pull the actuator downward and close off the flow channel, must also be determined for the following reasons. If the pressure force is comparable to or greater than the electric force, the periodic motions of the transducer actuators (i.e. tube deflections) are not straight forward to analyze. Fluid mechanical effects between transducers must be accounted for. If the electric force dominates, the tube deflections have the same periodicity as the applied magnetic traveling wave and approximate analysis of tube deflections is simple.

3.1 Pump Fluid Pressure Force

3.1.1 Theoretical Description Of The Pressure Force Exerted On The Transducer Actuator By The Pump Suction Head

The static fluid pressure exerted on the tube wall and the transducer actuator is a function of the suction head, H_s. Inertial

or fluid velocity effects on the fluid pressure will be neglected in the analysis.

$$P = \rho g H_s \tag{3.1}$$

The total fluid pressure force acting on each actuator is

$$f_p = P w l \tag{3.2}$$

$$= \rho g w l H_s \tag{3.3}$$

where w and l are dimensions from Figure 1.2.

Solve equation 3.3 for wl.

$$wl = \frac{f_p}{\rho g H_s} \tag{3.4}$$

wl is the variable area over which the fluid pressure acts on the actuator. It is a function of the gap width and will be derived experimentally in the next section. The emperical expression for wl would be used in describing the motion of the peristaltic pump, section 3.2, under operating conditions where the fluid pressure is comparable to the electric force.

3.1.2 Experimental Evaluation Of The Fluid Pressure Force

Figure 3.2 is a plot of the total force due to springs and

H_s (m)	M (kg)→	.297	.397	.497	.586	.675
	Mg (N)→	2.91	3.89	4.87	5.75	6.62
.05	$X - X_s$→ (m)	.00225	.00197	.00169	.00141	.00107
0.1		.00225	.00197	.00169	.00139	.00107
0.2		.00246	.00208	.00193	.00165	.00140
0.3		.00267	.00234	.00206	.00180	.00155
0.4		.00275	.00246	.00224	.00196	.00165
0.5		.00277	.00262	.00231	.00206	.00183
0.6		.00305	.00270	.00244	.00218	.00200

X_s = Tube Support Thickness
= .0017 meters

PRESSURE FORCE - GAP WIDTH DATA FOR VARIOUS PUMP SUCTION HEADS

Figure 3.1

PLOT OF SPRING FORCE, FLUID PRESSURE FORCE, AND COMBINED SPRING-FLUID PRESSURE FORCE VERSUS GAP WIDTH

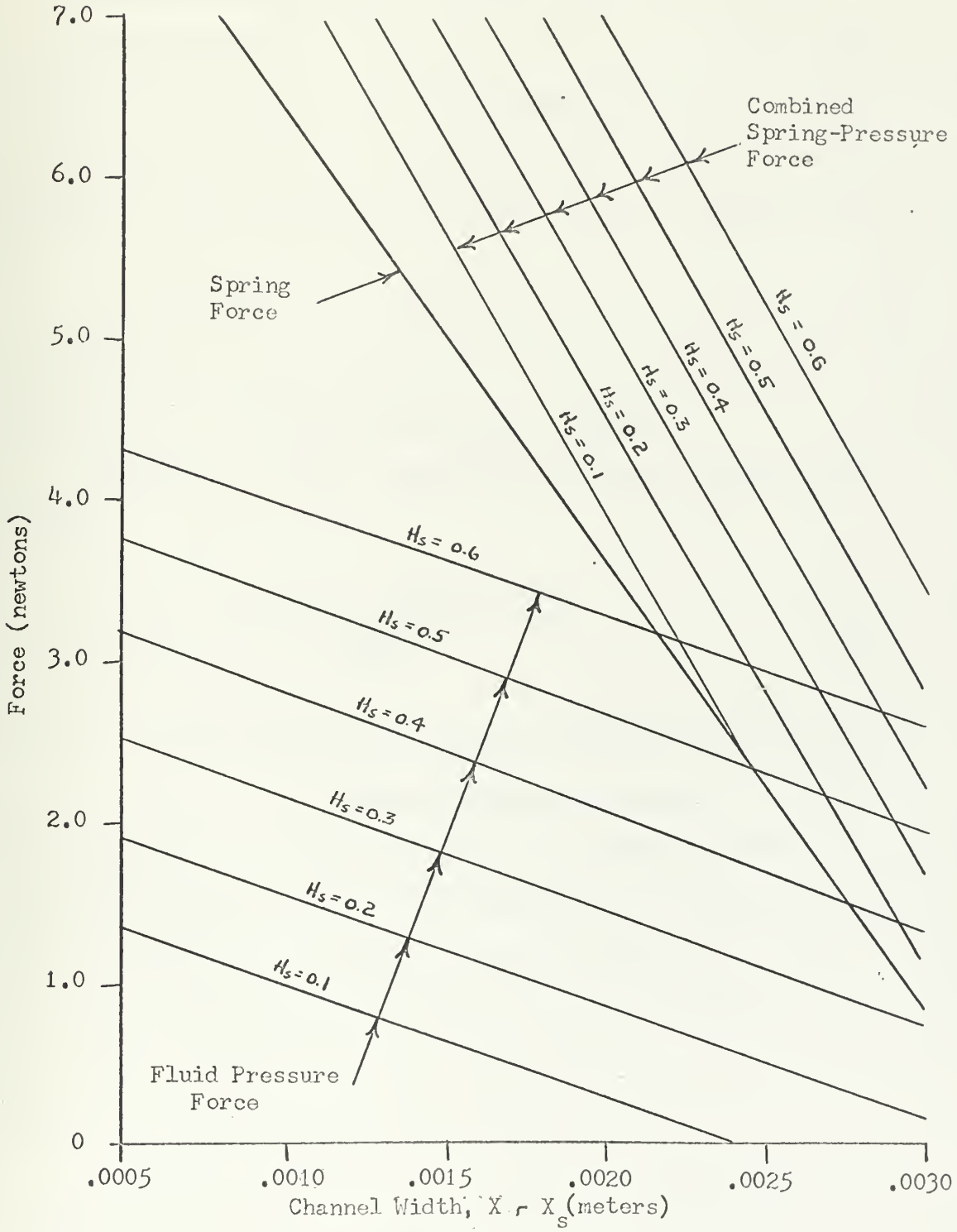

Figure 3.2

fluid pressure acting on each actuator versus channel width. Since the spring force is known, it is subtracted from the total force, leaving the force due to the fluid pressure alone. The fluid pressure curves yield an empirical expression for the fluid pressure force as a function of suction head and channel width.

$$f_p = 1.2 + 6\,H_s - 750\,(X - X_s) \qquad 3.5$$

where H_s and X are in meters and f_p is newtons.

Substitution of this empirical expression in equation 3.4 yields

$$wl = \frac{1.2 + 6\,H_s - 750\,(X - X_s)}{\rho g\,H_s} \qquad 3.6$$

3.1.3 Comparison Of Relative Magnitudes Of Forces Acting On The Transducer Actuator

The forces acting on the actuator vary with gap width, suction head, and exciter current. The fluid and spring forces act upward, while the weight of the actuator and the electric force act downward. During operation the gap width varies from about .004 to .0017 meters. Table 3.1 shows values of forces for different gap widths, suction heads, and exciter currents.

The figures in Table 3.1 do not clearly indicate what happens when the pump operates. As current to the exciter reaches its peak value, the actuator begins to close due to a net imbalance

Table 3.1

Approximate Force Values For Various Gap Widths

Force,(newtons)		X = .004	X = .003	X = .002	X = .0017
Fluid Pressure Force f_p, Figure 3.2	H_s=0.1	0.10	0.80	1.50	1.70
	H_s=0.2	0.65	1.35	2.05	2.25
	H_s=0.3	1.25	1.95	2.70	2.90
	H_s=0.4	1.85	2.55	3.30	3.50
Electric Force f_e, Figure 2.11	I=1.02	0.42	3.60	8.05	11.10
	I=1.50	0.91	7.75	17.50	24.00
Spring Force f_s, Figure 2.7		2.80	5.70	8.60	9.40
Actuator Weight Mg		2.91	2.91	2.91	2.91

of forces acting downward. As the actuator closes, the electric force increases at a rate greater than the spring and pressure forces combined. The actuator is unstable. Once it starts to close, the imbalance of forces increases and it will close completely. Further, as the channel pinches closed, all fluid is forced out and the fluid pressure drops to zero. Observation of operation of the pump shows that the fluid pressure and fluid dynamics do effect the pump, but that the electric force does dominate and the periodic motion of the actuators has the same frequency as the applied exciter current.

3.2 Theoretical Description Of Peristaltic Pump Motion[14,15]

The balance of forces acting on the actuators in Figure 1.2 yields

$$P\,(wl) + K\,(X_0 - X) = Mg + f_e \qquad 3.7$$

In static equilibrium, the weight is balanced by an equilibrium spring force.

$$K\,(X_0 - X_1) = Mg \qquad 3.8$$

Thus

$$P\,(wl) + K\,(X_1 - X) = f_e \qquad 3.9$$

Rearrange equation 3.9 and divide by wl.

$$P = \frac{f_e}{wl} - \frac{K\,(X_1 - X)}{wl} \qquad 3.10$$

Substitute for f_e from equation 2.27 and for wl from equation 3.6.

$$P = \frac{\rho g H_s}{1.2 + 6h - 750X}\left[\mu_0 N^2 abd^2 \frac{I^2}{X^2} - K\,(X_1 - X)\right] \qquad 3.11$$

Consider the tube wall to be a continuously deforming surface excited by a traveling wave. That is, the discrete motions of the transducer actuators are approximated as an appropriate continuous traveling wave.

The tube wall deflection travels to the right in Figure 3.3 with a constant velocity, c, which is a function of the frequency and wavelength of the traveling wave.

CROSS SECTIONAL VIEW OF THE PERISTALTIC PUMP IN THE FIXED AND MOVING FRAMES

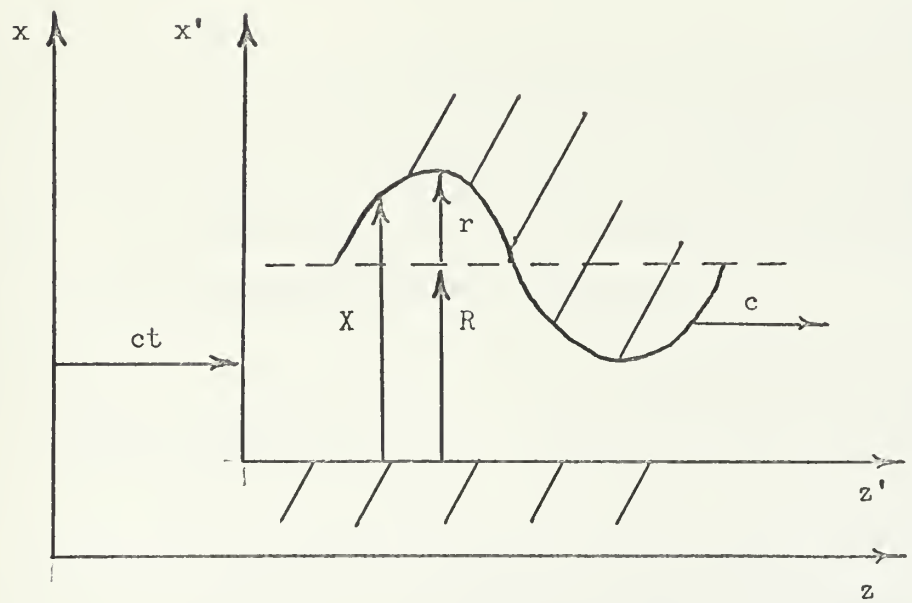

$$x = x'$$

$$z = z' + ct$$

$$P' = P'(z)$$

$$V' = V'_z(x)$$

$$r = r(z')$$

Figure 3.3

$$c = \lambda f \qquad 3.12$$

where $\lambda = 41$ from Figure 1.2

The tube wall itself is fixed in longitudinal position and moves only transversely. The tube wall position in the wave or moving frame of reference is

$$X = R + r(z') \qquad 3.13$$

In the wave frame, the traveling wave is a periodic stationary deflection. By assuming steady state flow conditions and ignoring inertia, the Navier-Stokes fluid flow equation is

$$\nabla P = \mu \nabla^2 v \qquad 3.14$$

The model for the tube or channel is quasi one dimensional. The pressure is independent of transverse position. The velocity is purely in the longitudinal direction, but varies with transverse position.

$$\frac{d P'}{dx'} = 0 \qquad 3.15$$

$$\frac{d P'}{dz'} = \mu \frac{d^2 v_z'}{dx'^2} \qquad 3.16$$

In the wave frame of reference, the volume rate of flow

per unit depth in the y direction is

$$Q' = \int_0^X v_z' \, dx \qquad 3.17$$

The fluid velocity is determined by integrating equation 3.16 and applying the boundary conditions

$$v_z' \, (x = X) = v_z \, (x = X) - c = -c \qquad 3.18$$

$$v_z' \, (x = 0) = -c \qquad 3.19$$

The result is

$$v_z' = \frac{1}{2\mu} \frac{dP}{dz'} (x^2 - Xx) - c \qquad 3.20$$

Substitute equation 3.20 in equation 3.17 and integrate to determine the expression for flow rate.

$$Q' = - \frac{1}{12\mu} \frac{dP}{dz'} X^3 - cX \qquad 3.21$$

Rearrange and solve for the pressure gradient.

$$\frac{dP}{dz'} = - \frac{12\mu}{X^3} (Q' + cX) \qquad 3.22$$

Now solve for the time average flow rate in the fixed frame

with the ultimate object of obtaining an expression for the flow rate in the moving frame for substitution in equation 3.22.

$$\langle Q \rangle = \left\langle \int_0^X v_z \, dx \right\rangle \qquad 3.23$$

$$= \left\langle \int_0^X (v_z' + c) \, dx \right\rangle \qquad 3.24$$

The first part of the integral is Q'. The second is the phase velocity times R, the time average value of X.

$$\langle Q \rangle = Q' + cR \qquad 3.25$$

Rearrange.

$$Q' = \langle Q \rangle - cR \qquad 3.26$$

which is independent of longitudinal position. Substitute Q' in equation 3.22 and note that $c\,(X - R) = cr$.

$$\frac{dP}{dz'} = - \frac{12\mu}{X^3} (\langle Q \rangle + cr) \qquad 3.27$$

The expression for pressure from equation 3.10 can be differentiated with respect to z, since $\frac{d}{dz} = \frac{d}{dz'}$, to yield

$$- \frac{12\mu}{X^3} (\langle Q \rangle + cr) = \frac{d}{dz} \left[\frac{f_e}{wl} - \frac{K (X_1 - X)}{wl} \right] \qquad 3.28$$

For a given periodic driving current, equation 3.28 represents a non-linear equation which can be solved for X. Only one boundary condition is required. The response desired is periodic with the same wavelength as the driving current. The required solution for X is found by adjusting the boundary condition at one position such that the deflection returns to the same value after one wavelength, that is , $X(z') = X(z' + \lambda)$.

3.3 Determination Of Pressure-Flow Characteristics For A Known Transducer Actuator Deflection

3.3.1 Description Of Peristaltic Traveling Wave Deflections

The peristaltic pump developed for this thesis, as stated in section 3.1.3, operates so that electric forces dominate. The traveling wave frequency is the same as the applied electric exciter frequency. The transducers come very close to operating as open-close relays. Thus, an approximate description of the tube deflection is known. The non-linear equation 3.28 need not be solved to determine X. Rather, the pressure-flow characteristic for the pump can be determined by integrating equation3.27 under the assumption that all quantities inside the integral are known functions of z.

Figure 3.4 is a Sanborn Recording of the tube deflections during pumping. This figure can be compared to Figure 2.15c, a similar trace except that no fluid filled tube is in the transducers. The erratic traces on Figure 3.4 are due to sensitivity adjustment difficulties on the recorder, not fluid action. The presence of

SANBORN RECORDER PLOTS OF TRANSDUCER ACTUATOR MOTION VERSUS TIME

DURING PERISTALTIC PUMPING

I_{dc} = 10.0 @ 26 turns
= 0.52 @ 500 turns
i_{ac} = 0.50 cos wt

Frequency = 0.33

H_s = 10 cm.
H_d = 10 cm.
Flow Rate = 42.5×10^{-8} m^3/sec

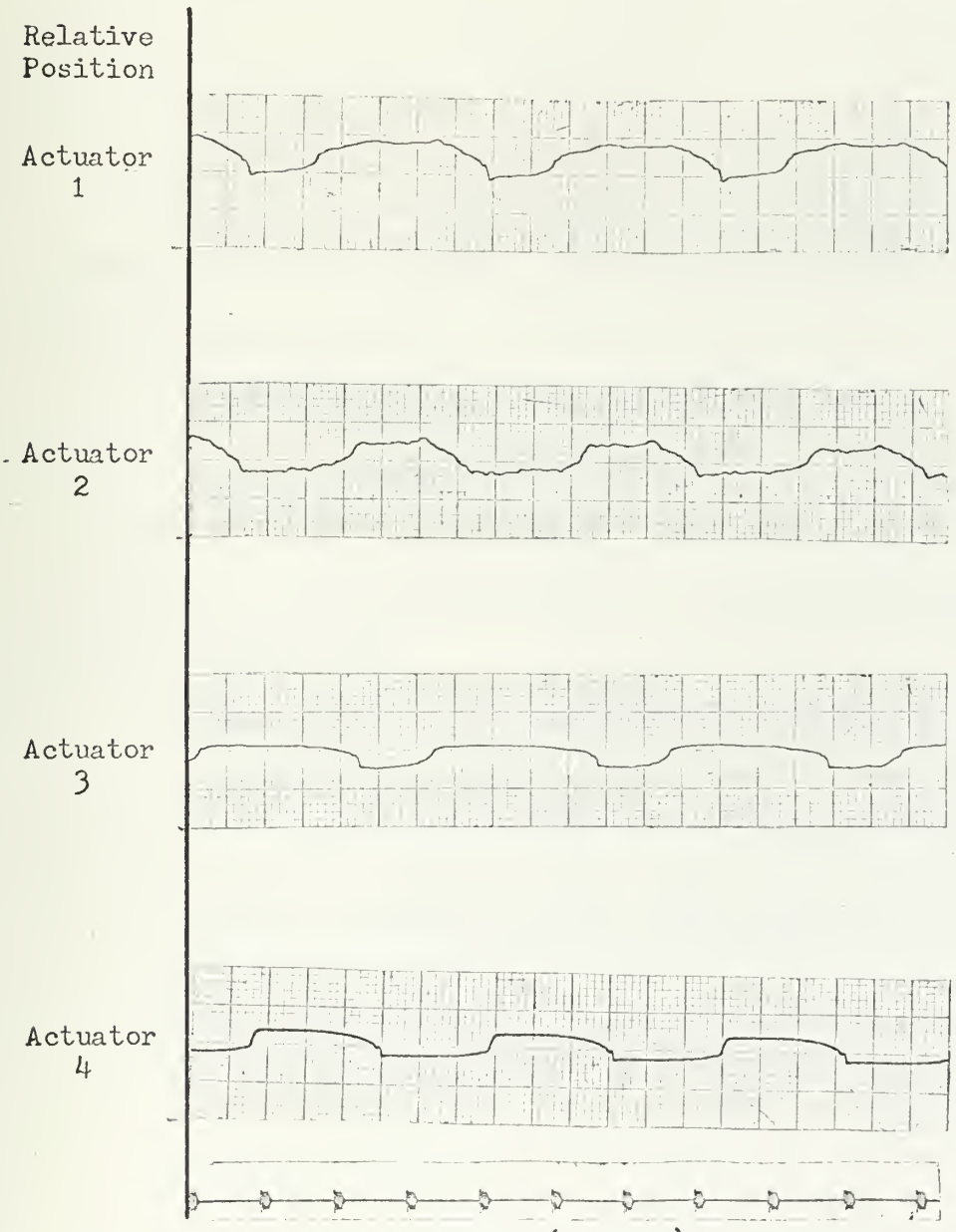

Figure 3.4

fluid does not significantly change the traveling wave.

$$\Delta P_\lambda = \int_o^\lambda \frac{dP}{dz}\, dz \qquad 3.29$$

$$- 12\mu \int_o^\lambda \frac{\langle Q \rangle + cr}{X^3}\, dz \qquad 3.30$$

The peristaltic traveling wave can be approximated as a square wave or as a sine wave. Both approximations are made in succeeding sections.

3.3.2 Square Traveling Wave Approximation To Peristaltic Pumping[16]

The peristaltic traveling wave can be approximated as a square wave. This is illustrated in the laboratory and wave frames in Figure 3.5.

The pressure rise over a wavelength for a square wave is determined geometrically using equation 3.30.

$$\Delta P_\lambda = - 12\mu \left[\frac{\langle Q \rangle + cr}{(R + r)^3} + \frac{\langle Q \rangle - cr}{(R - r)^3} \right] \frac{\lambda}{2} \qquad 3.31$$

Normalize this equation by letting

$$h = \frac{r}{R} \qquad 3.32$$

$$\underline{\langle Q \rangle} = \frac{\langle Q \rangle}{Rc} \qquad 3.33$$

$$\underline{\Delta P} = \frac{R^2 \Delta P_\lambda}{6 \mu \lambda c} \qquad 3.34$$

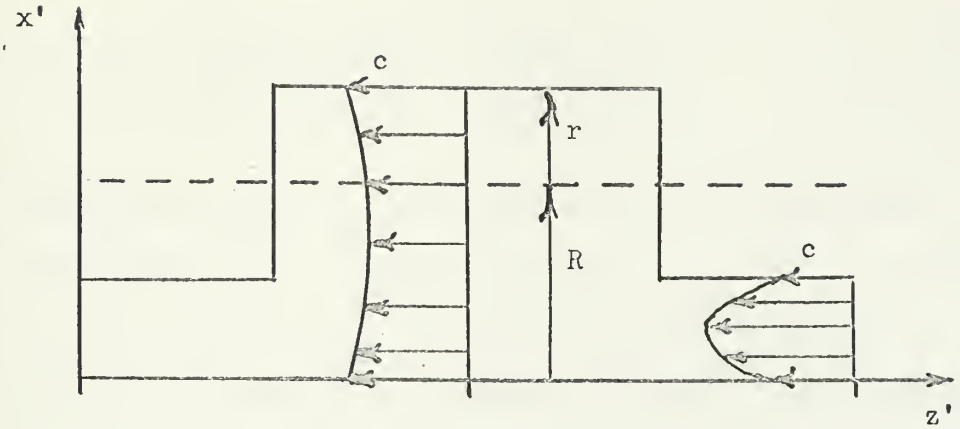

a. Square wave deflection in the moving frame. The wall velocity is -c and the volume flow rate is independent of z'.

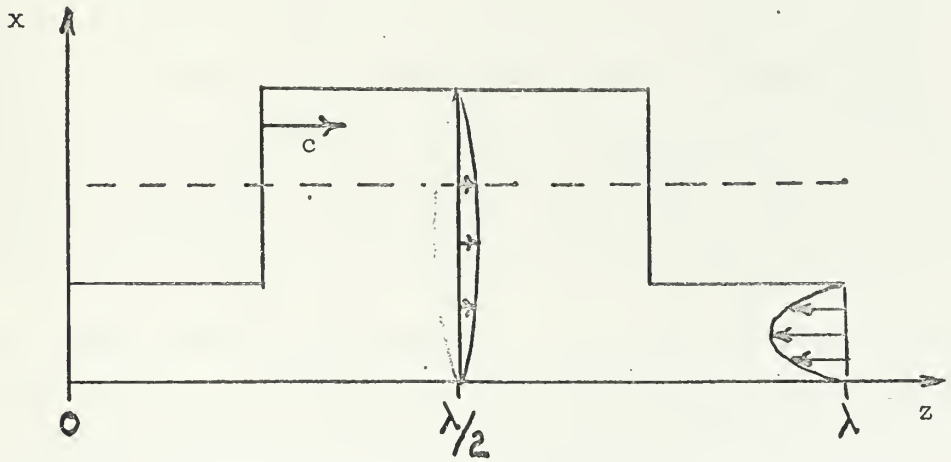

b. Square wave deflection in the fixed frame. The increasing volume in the half wavelength between $\lambda/2$ and λ necessitates a net flow into that volume. The velocity profiles would yield a net flow out of the decreasing volume between 0 and $\lambda/2$.

Figure 3.5

Substitute these values in equation 3.31.

$$-\underline{\Delta P} = \left[\frac{\langle Q\rangle + h}{(1+h)^3}\right] + \left[\frac{\langle Q\rangle - h}{(1-h)^3}\right] \qquad 3.35$$

The normalized pressure rise as a function of normalized time average flow rate is plotted in Figures 3.6, 3.7, 3.8, and 3.9 for various values of h. As h approaches one, the channel is cutoff and the pressure rise becomes infinite. Such a positive displacement pump, operating so the channel is cut off while pumping, can theoretically pump against an infinite head.

When h is zero, there is no channel wall deflection. If a flow rate existed in the channel, this case would give the pressure rise up the channel for a given flow rate with no wall deflection. However, in the specific case of the peristaltic pump where all flow is due to wall motion, the flow rate and pressure rise would also be zero.

The intercept points for the normalized pressure-flow curves are determined by evaluating the normalized pressure rise for zero flow rate and the normalized time average flow rate for zero pressure rise. Intercept values for operating suction heads and normalized channel width variations are shown in Table 3.2.

$$\underline{\Delta P_0} = \left[\frac{1}{(1-h)^3} - \frac{1}{(1+h)^3}\right] h \qquad 3.36$$

$$\underline{\langle Q\rangle_0} = \left[\frac{(1+h)^3 - (1-h)^3}{(1+h)^3 + (1-h)^3}\right] h \qquad 3.37$$

Table 3.2

Square Wave Pressure-Flow Intercepts

Figure	H_s	h	ΔP_0	$\langle Q \rangle_0$
3.7	10	.131	.111	.049
3.8	20	.172	.196	.082
3.9	30	.214	.321	.122
3.10	40	.228	.374	.137

3.3.3 Sinusoidal Traveling Wave Approximation To Peristaltic Pumping[17]

The peristaltic traveling wave can also be approximated as sinusoidal. This is illustrated in Figure 3.6. The pressure rise over a wavelength for a sinusoidal traveling wave is determined by integration of equation 3.30.

$$\Delta P_\lambda = \frac{12\mu}{k} \int_0^\lambda \frac{\langle Q \rangle + cr \cos(wt - kz)}{[R + r \cos(wt - kz)]^3} \; (-k\, dz) \qquad 3.38$$

When solved[18], this integral becomes

$$\Delta P_\lambda = \frac{6\mu\lambda}{(R^2 - r^2)^{5/2}} \left[3cRr^2 - \langle Q \rangle (2R^2 + r^2) \right] \qquad 3.39$$

Normalize equation 3.39 using the same normalization as in the previous section. Then

$$\underline{\Delta P} = \frac{h^2}{(1 - h^2)^{5/2}} \left[3 - \frac{2 + h^2}{h^2} \underline{\langle Q \rangle} \right] \qquad 3.40$$

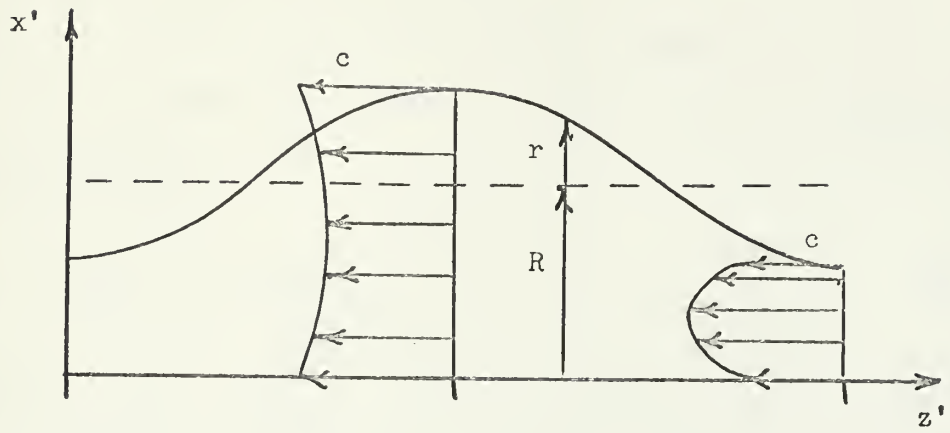

a. Sinusoidal wave deflection in the moving frame. The wall velocity is -c and the volume flow rate is independent of z'.

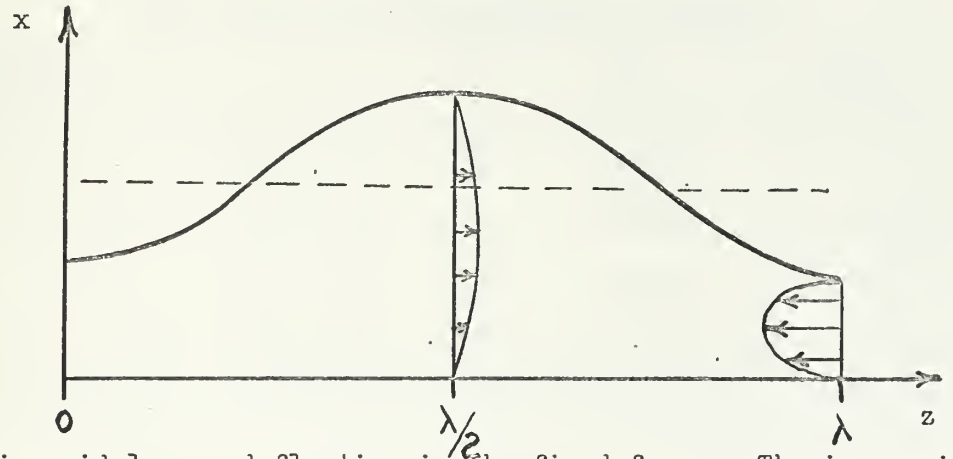

b. Sinusoidal wave deflection in the fixed frame. The increasing volume in the half wavelength between $\lambda/2$ and λ necessitates a net flow into that volume. The velocity profiles would yield a net flow out of the decreasing volume between 0 and $\lambda/2$.

Figure 3.6

The discussion in the previous section is applicable to the sinusoidal approximation of the peristaltic traveling wave. As from the previous section, the intercept points for Figures 3.7, 3.8, 3.9, and 3.10 are below. Specific values of the points are in Table 3.3.

$$\underline{\Delta P_0} = \frac{3h^2}{(1 - h^2)^{5/2}} \qquad 3.41$$

$$\underline{\langle Q \rangle_0} = \frac{3h^2}{2 + h^2} \qquad 3.42$$

Table 3.3

Sinusoidal Wave Pressure-Flow Intercepts

Figure	H_s	h	ΔP_0	$\langle Q \rangle_0$
3.6	10	.131	.0544	.0256
3.7	20	.172	.0956	.0438
3.8	30	.214	.1550	.0672
3.9	40	.228	.1784	.0760

3.3.4 Experimental Pump Operation

The pump was operated peristaltically with the same suction head and normalized channel width combinations for which pressure-flow characteristics were determined in sections 3.3.2 and 3.3.3. Values of pump flow rates and pressure heads were measured and are recorded in Appendix I. The operating points are plotted on the appropriate pressure-flow curve, Figure 3.7, 3.8, 3.9, or 3.10.

NORMALIZED PRESSURE-FLOW CHARACTERISTIC FOR PERISTALTIC PUMPING

$h = 0.131$
$H_s = 0.1$ m.

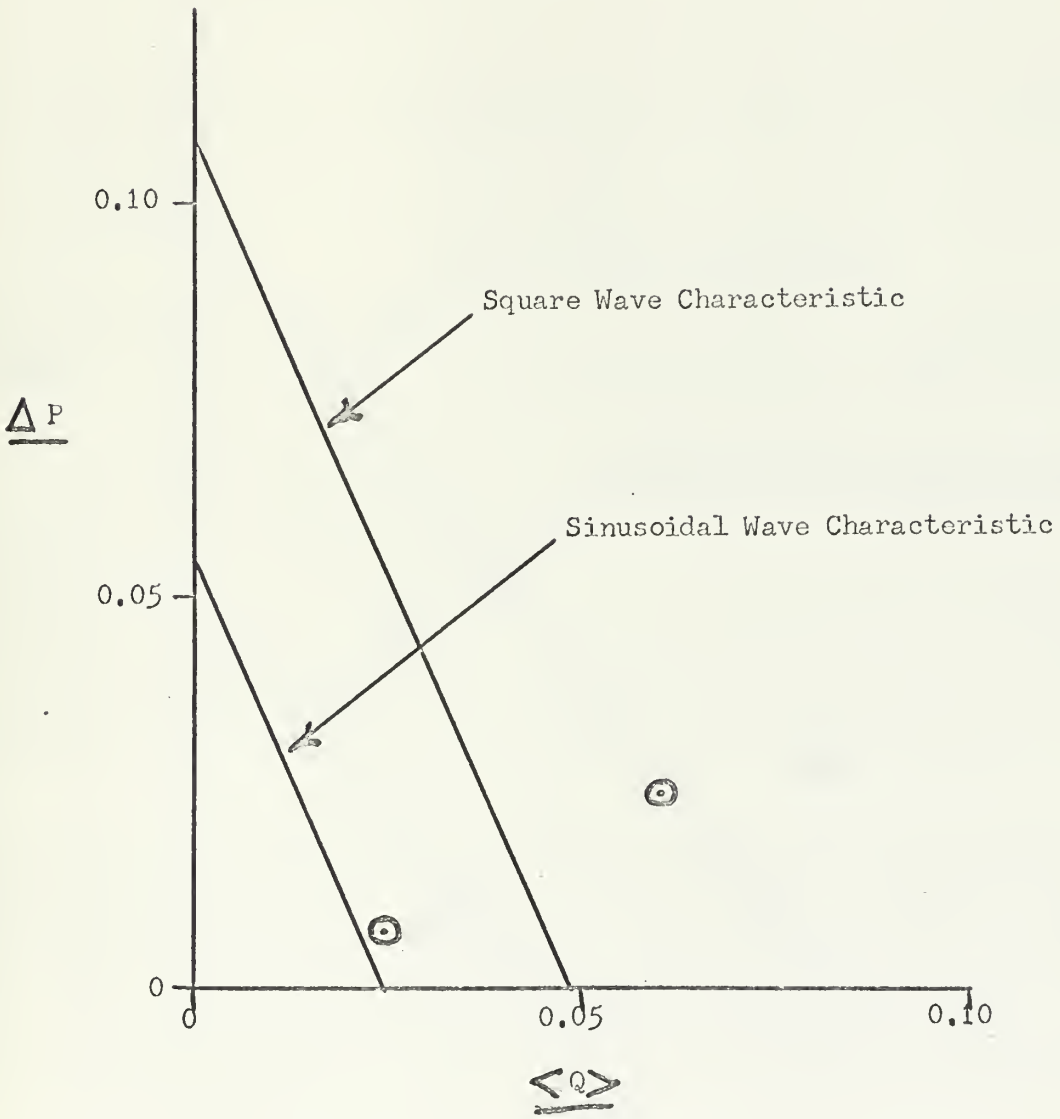

Figure 3.7

NORMALIZED PRESSURE-FLOW CHARACTERISTIC FOR PERISTALTIC PUMPING

$h = 0.172$
$H_s = 0.2$ m.

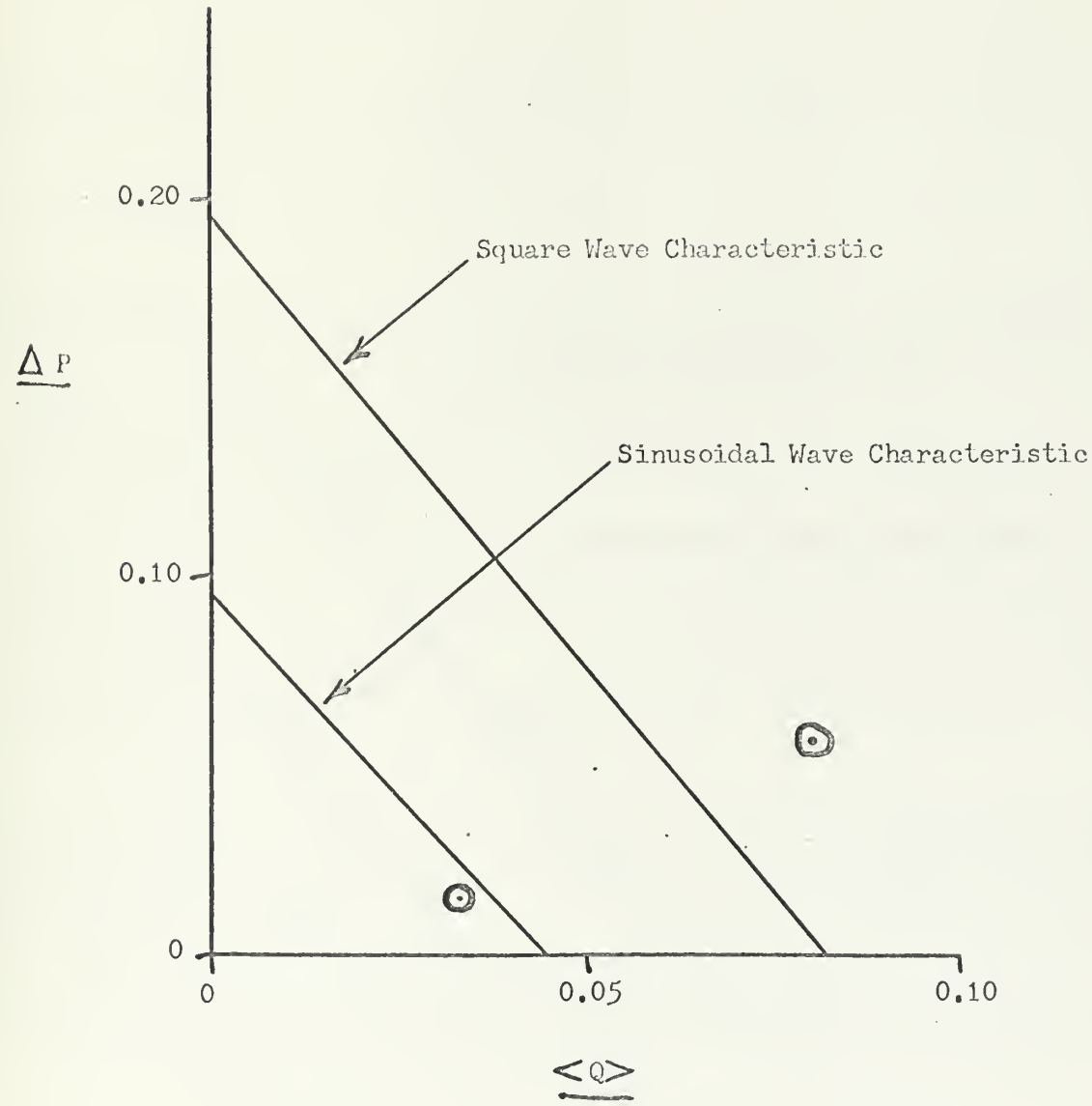

Figure 3.8

NORMALIZED PRESSURE-FLOW CHARACTERISTIC FOR PERISTALTIC PUMPING

$h = 0.214$
$H_s = 0.3$ m.

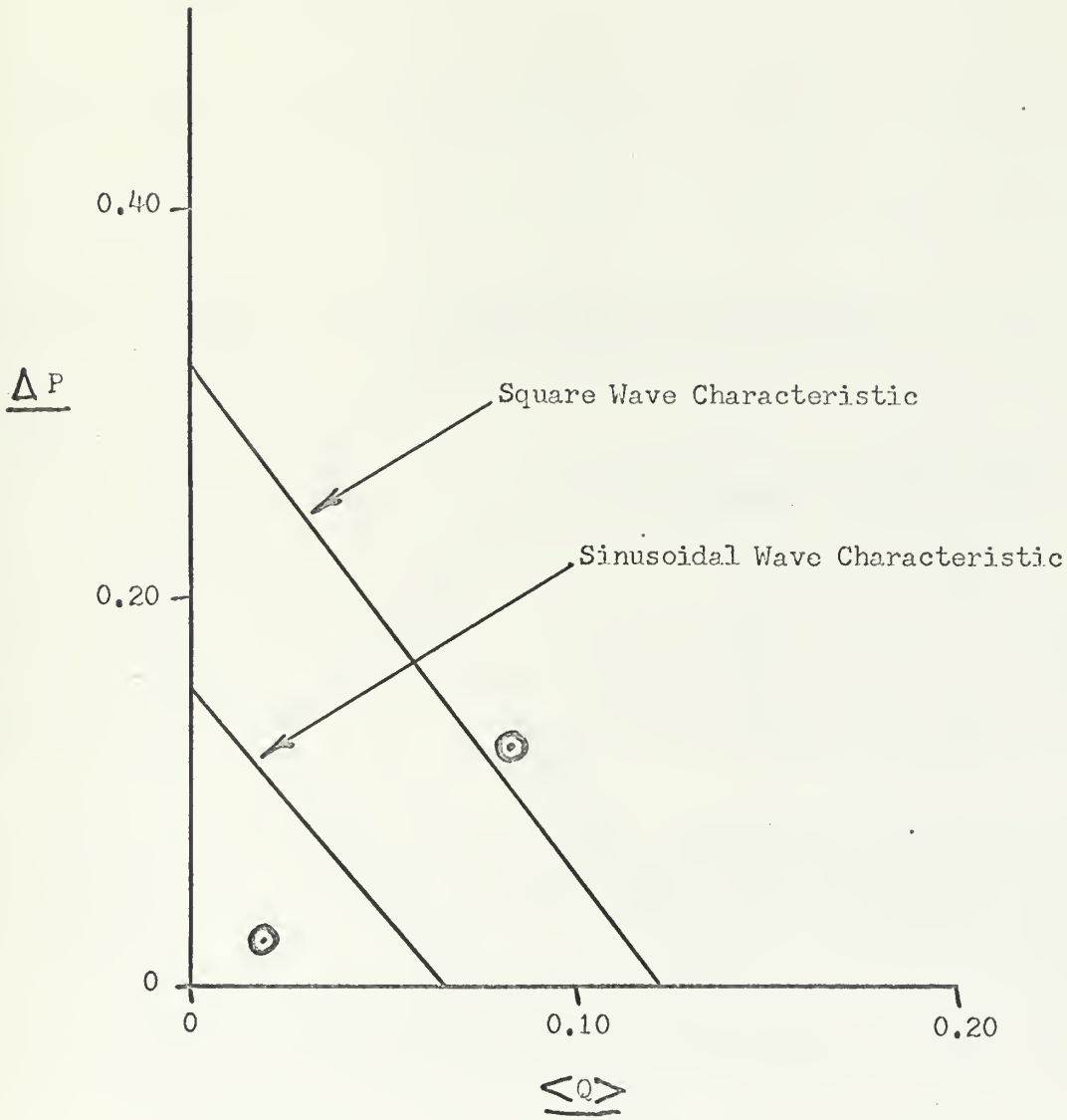

Figure 3.9

NORMALIZED PRESSURE-FLOW CHARACTERISTIC FOR PERISTALTIC PUMPING

$h = 0.228$
$H_s = 0.4$ m.

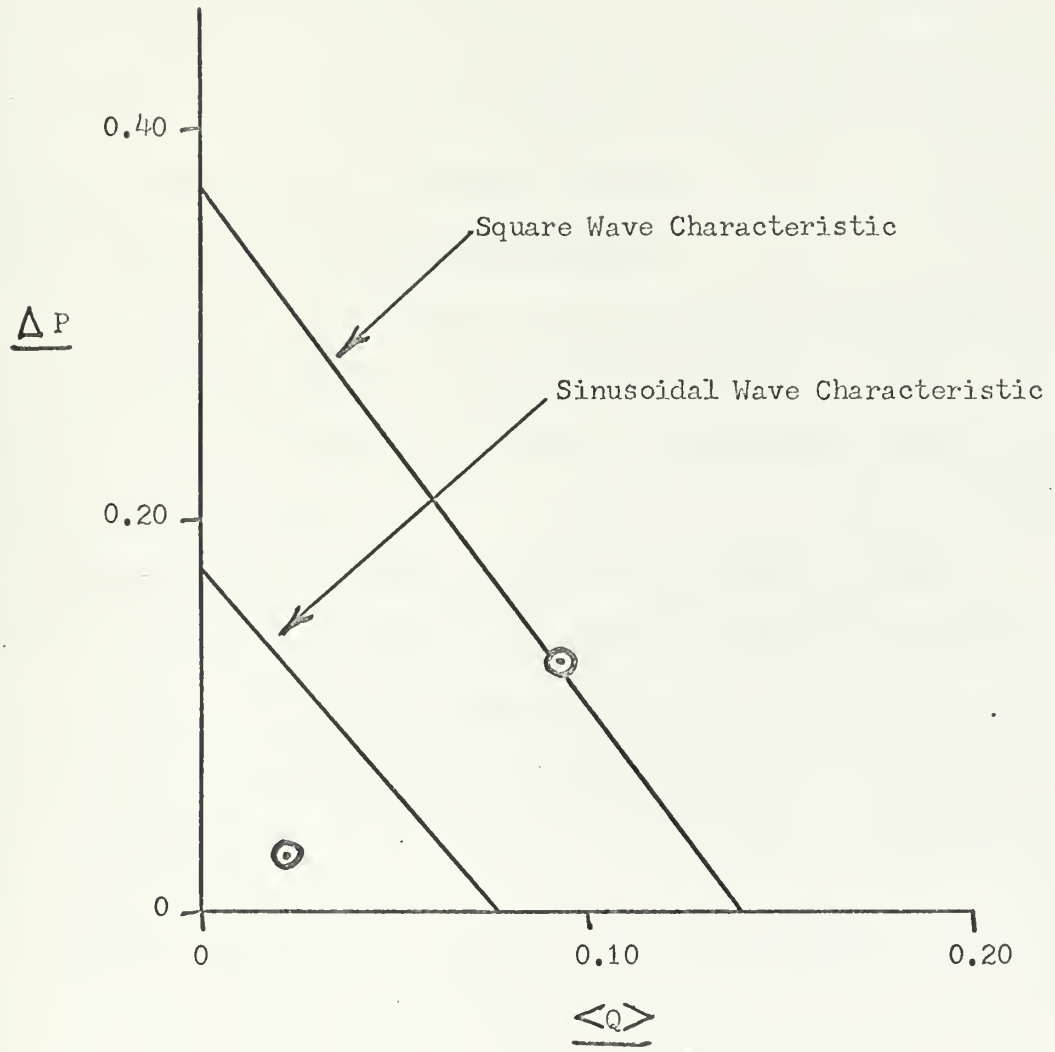

Figure 3.10

In Appendix I, the measured flow rate was divided by the channel width prior to normalization to obtain flow per unit channel width. The pump pressure differential was determined by measuring a static height difference between the pump suction and discharge headers. The normalized flow and pressure differential are determined using the same definitions as in sections 3.3.2 and 3.3.3 and applying the measured parameters of frequency, wavelength, channel width, and phase velocity.

3.3.5 Cut Off Or Occluded Pumping

As was pointed out in section 3.3.2, when h = 1, the channel is cut off during pumping and theoretically the pump can pump against an infinite head. In this case, a pressure-flow characteristic is meaningless.

Theoretically, the entire contents of the pump are pushed forward at the phase velocity of the applied traveling wave during occluded pumping. For a unit tube width,

$$\langle Q \rangle = Rc \qquad 3.44$$

Using the same definition for normalized time average flow rate as in section 3.3.2,

$$\underline{\langle Q \rangle} = \frac{\langle Q \rangle}{Rc} \qquad 3.45$$

$$= \frac{\langle Q \rangle_{measured}}{\langle Q \rangle_{theoretical}} \qquad 3.46$$

$\langle Q \rangle$ can range from zero, no flow, to one, perfect occlusion. The experimental normalized time average flow rate in Appendix II ranged from 0.26 to 0.45. Considering the sources of error, which will be mentioned in section 3.4, the most important to inefficient occluded pumping are improper time phasing between actuators and the fact that the pump consists of only one wavelength. Both of these items bring about physical conditions under which the entire contents of the tube under each actuator are not pushed forward as the actuator squeezes downward.

If the pump were operated so that each transducer was on or off, almost ideal occlusion could be obtained if each actuator was held down until the succeeding one was closed. Under these circumstances, the fluid has no choice except to move onward.

For the specific pump in this thesis and under the type of operation finally used where maximum current was applied for all pumping, peristaltic and occluded, occlusion is the most efficient form of pumping. For a given power input, occlusion gives the greatest flow rate. Unless less than fully occluded pumping is desired, the most effective pump would be built to operate fully occluded.

3.3.6 Reynold's Number

The appropriate Reynold's number describing flow in the peristaltic pump has been shown to be[19]

$$Re = \frac{R^2 c}{\nu \lambda} \qquad 3.43$$

The Reynold's number varies between 1.31 and 8.65 for the operating points of the pump. Exact values are shown in Appendices I and II. In each case, inertial forces are greater than viscous forces. In spite of this, the viscous model developed yields reasonably accurate results.

3.4 Sources of Error

It is difficult to attribute the error between theoretical pressure-flow characteristics and experimental operating points to any single cause. The inertial nature of the pump, which is not accounted for in the theoretical model, could cause some error. The mechanical aspects of pumping could have produced errors. The rubber pump tube was somewhat elastic which could have altered flow. The tube was eliptical in shape rather than a square channel as the theory assumes. The model assumes the vertical walls of the tube are always vertical and perfectly elastic to up and down motions, while the channel is of constant width. The real pump has elastic vertical walls which bow out. Channel width varies as the pump actuator moves up and down. As was pointed out in section 2.5, perfect ninety degree phase shifting between transducers was not obtained. The uneven actuator motion could have affected flow. The pump pressure head, from which ΔP results, is on the order of one millimeter. Accurate measurement of these differentials was difficult. The pump has rather long sections of flexible tube on the inlet and outlet. The flow resistance and surface tension effects at the ends of

these tubes could alter pressure-flow relations.

Considering the sources of error, it is surprising that the operating points are as close to the theoretical pressure-flow curves as they are. But, the real value of the project is not the relative agreement between theory and experiment. Its value is in the physical realization that longitudinal peristaltic type flow can be produced by purely vertical transducer motion. No longitudinal mechanical motion is involved.

CHAPTER IV

CONCLUSIONS

The experimental work done in this thesis has shown that the observed peristaltic pump operating points lie reasonably close to the theoretical pressure-flow characteristics of the pump. It has not been shown that the pressure-flow characteristics accurately predict pump operation. First, very few operating points were measured. No real trend or correlation between measured and theoretical operation could be observed. Second, the large number of error sources make it difficult to differentiate flow variations due to theoretical prediction from flow variations due to experimental error. The exception to this is occluded pumping. Complete occlusion theory predicts a normalized flow rate of one. Flow rates less than one are due to inefficient or improper experimental operation of the pump and are readily recognizable.

The thesis and experimental work have been of value. The major reason for the effort was to show that peristaltic pumping could be produced by a principle which had never been tried. Longitudinal flow was produced where no longitudinal mechanical motion was involved. The importance of this fact cannot be over emphasized. The longitudinally traveling peristaltic wave was produced by properly phasing the transverse motion of discrete electromechanical transducers. If a peristaltic pump is ever to be miniaturized and used as a replacement for an organ in the

body, the use of some sort of mechanical roller is not practical. But, such a pump could be designed, using the principles of this thesis, which would be easy to miniaturize, mechanically simple, flexible, light weight, compact, and reliable. For instance, if very small displacements are desired, the transverse transducer motion could be produced by piezoelectric expansion of ceramic crystals. The excitation for a piezoelectric crystal is a voltage applied across it.

Another new principle developed in this work is the direct relationship between the applied electric force and the transverse motion of the transducer actuator. In the case of the peristaltic pump developed in chapters two and three, the magnitude of the electric force is inversely proportional to the gap width squared. In future peristaltic devices, it might be desirable to utilize the electric force or the magnetic field directly to produce fluid motion. This has possibilities in pumping magnetic liquids directly or in pumping by means of magnetic liquids. A traveling magnetic wave might be made to pull magnetic liquid along just as the traveling field of a motor pulls the armature along. Both of these principles are of value for future experimental work.

The specific pump developed could be improved in the following ways. For most efficient operation, it should pump by totally cutting off the flow channel in its transverse motions. This causes the greatest volume flow rate for power input. However, total occlusion could be disadvantageous. Blood is very sensitive

to pumping. The effect of being pinched in the flow channel could damage blood so that it might not be usable. The pump should be improved for pumping both fully occluded and peristaltically. Phasing and phase sequencing need improvement. Proper application of excitation could produce rhythmic heart-beat-like pumping rather than continuous smooth flow, if that were desired. Since the transducers act almost like on-off relays, a complex sinusoidal excitation is not needed. More efficient, simpler excitation, which would be just as effective, could be provided by a DC on-off power source.

One of the most serious defects in the pump is the low volume flow rate. The pump tube used was a long, thin balloon. It was difficult to find an elastic tube which would fit in the gap between the actuator and the exciter and which did not exhibit elastic forces opposing gap close off greater than the electric forces applied. Ideally, a long, very flexible, broad tube is needed which would fill more of the channel width and have negligible vertical wall rigidity. Total channel "elasticity" should be due to the suction height of the fluid in the channel.

The type of electromechanical peristaltic pump investigated in this thesis is rugged, inexpensive, and simple. It was built using common transformers, springs, plastic, and balloons. The pump operated consistently and dependably. These features , and those already mentioned, make it worth additional development.

H_s	f	c	h	$\langle Q \rangle$	Δh	ΔP_λ	$\frac{\Delta P}{}$	$\frac{\langle Q \rangle}{}$	Re
m.	c/s	m/s	r/R	flow m^3/s	m.	g h	$\frac{R^2 \Delta P_\lambda}{6\mu\lambda c}$	$\frac{\langle Q \rangle / w}{Rc}$	$\frac{R^2 c}{\nu \lambda}$
10	0.33	.0925	0.131	11×10^{-8}	.001	9.8	.025	.06	1.31
10	1.10	.308	0.131	15×10^{-8}	.001	9.8	.0075	.0245	4.35
20	0.33	.0925	0.172	15.5×10^{-8}	.002	19.3	.055	.08	1.44
20	1.30	.364	0.172	24.5×10^{-8}	.002	19.3	.014	.0329	5.68
30	0.33	.0925	0.214	16.7×10^{-8}	.004	39.2	.122	.0825	1.60
30	1.80	.500	0.214	21×10^{-8}	.003	29.6	.023	.0191	8.65
40	0.33	.0925	0.228	19×10^{-8}	.004	39.2	.127	.0915	1.66
40	1.50	.420	0.228	21.4×10^{-8}	.004	39.2	.028	.0223	7.53

$\lambda = 0.28$ m.

$\mu = 10^{-3}$ N-sec/m^2

$w = 10^{-2}$ m.

$\rho = 10^3$ kg/m^3

$\nu = 10^{-6}$ m^2/sec.

Peristaltic Pumping Data

APPENDIX I

H_s	f	c	h	$\langle Q \rangle$	$\underline{\langle Q \rangle}$	Re
m.	c/s	m/s	r/R	m^3/s	$\frac{\langle Q \rangle / w}{Rc}$	$\frac{R^2 c}{\nu \lambda}$
10	0.33	.0925	1.00	44×10^{-8}	.425	0.45
10	0.70	.196	1.00	79×10^{-8}	.360	0.87
20	0.33	.0925	1.00	49×10^{-8}	.431	0.50
20	0.90	.252	1.00	123×10^{-8}	.400	1.36
30	0.33	.0925	1.00	52×10^{-8}	.423	0.58
30	1.30	.364	1.00	127×10^{-8}	.262	2.30
40	0.33	.0925	1.00	57×10^{-8}	.450	0.62
40	1.20	.336	1.00	209×10^{-8}	.454	2.25

$\lambda = 0.28$ m. $\rho = 10^3$ kg/m^3

$\mu = 10^{-3}$ N-sec/m^2 $\nu = 10^{-6}$ m^2/sec.

$w = 10^{-2}$ m.

Occluded Pumping Data

APPENDIX II

REFERENCES

1. Burns, J.C. and Parks, T., "Peristaltic Motion," Journal of Fluid Mechanics, 1967, Vol. 29, Part 4, p. 731-743

2. Hanin, M., "The Flow Through A Channel Due To Transversely Oscillating Walls," Israel Journal of Technology, Vol. 6, No. 1-2, 1968, p. 67-71

3. Shapiro, A.H., Jaffrin, M.Y., and Weinberg, S.L., Peristaltic Pumping With Long Wave Lengths At Low Reynold's Number, Publication No. 68-5, Fluid Mechanics Laboratory, Department of Mechanical Engineering, Massachusetts Institute of Technology, Cambridge, Massachusetts, September, 1968

4. Melcher, J.R., Continuum Electromechanics Course 6.528 Notes, Massachusetts Institute of Technology, Cambridge, Massachusetts, 1969

5. Shapiro, p. 6-7

6. Shapiro, p. 33

7. Shapiro, p. 7

8. Melcher, p. 10.7.1

9. Woodson, H.H. and Melcher, J.R., Electromechanical Dynamics, John Wiley and Sons, New York, London, and Sydney, 1968, p. 22-23

10. Woodson, p. 67

11. Woodson, p. 422

12. Melcher, p. 10.8.3

13. Woodson, p. 185-186

14. Shapiro, p. 7-10

15. Melcher, Section 10.7 and 10.8

16. Melcher, p. 10.7.4

17. Shapiro, p. 10

18. Gadshteyn, I.S. and Ryzhik, I.M., Tables of Integrals, Series, and Products, 4th Edition, Academic Press, New York and London, 1965, p. 148

19. Shapiro, p. 33

Thesis
B8837 Burn
118369
Electromechanical
peristaltic pumping.